

Chapter 1

Dissipative Kerr solitons in optical microresonators*

TOBIAS HERR^{1,2}

MICHAEL L. GORODETSKY^{3,4}

TOBIAS J. KIPPENBERG¹

Abstract: This chapter describes the discovery and stable generation of temporal dissipative Kerr solitons in continuous-wave (CW) laser driven optical microresonators. The experimental signatures as well as the temporal and spectral characteristics of this class of bright solitons are discussed. Moreover, analytical and numerical descriptions are presented that do not only reproduce qualitative features but can also be used to accurately model and predict the characteristics of experimental systems. Particular emphasis lies on temporal dissipative Kerr solitons with regard to optical frequency comb generation where they are of particular importance. Here, one example is spectral broadening and self-referencing enabled by the ultra-short pulsed nature of the solitons. Another example is dissipative Kerr soliton formation in integrated on-chip microresonators where the emission of a dispersive wave allows for the direct generation of unprecedentedly broadband and coherent soliton spectra with smooth spectral envelope.

1.1 Introduction to optical microresonator Kerr-frequency combs

Ultra high quality-factor (Q) optical whispering-gallery mode resonators have long been considered promising for their nonlinear optical properties since their

*To appear in *Nonlinear optical cavity dynamics*, ed. Ph. Grell

¹École Polytechnique Fédérale de Lausanne (EPFL), CH-1015 Lausanne, Switzerland

²Centre Suisse d'Électronique et de Microtechnique (CSEM), Neuchâtel, Switzerland

³Faculty of Physics, M. V. Lomonosov Moscow State University, Moscow, Russia

⁴Russian Quantum Center, Skolkovo, Russia

discovery by Braginsky and co-workers in 1989 [1]. Early works included the observation of bistability, thermal nonlinearity[2], Kerr-nonlinearity at cryogenic temperature[3], stimulated Raman- [4] and Brillouin-scattering[5], electro-optic effect[6, 7], as well as second[8] and third[9] harmonic generation. In particular, the third order Kerr-nonlinearity can give rise to parametric oscillations in an optical microresonator. In this four-photon process two pump photons are converted to one signal and one idler photon (i. e. degenerate four-wave mixing) where the photonic energy is conserved. These parametric oscillations (sometimes called hyper-parametric to distinguish them from three-photon oscillations associated with the second order optical nonlinearity), despite being well-known in nonlinear optics for decades[10], were observed in ultra high-Q toroidal fused silica and crystalline resonators only in 2004[11, 12]. These studies demonstrated the dramatic reduction of threshold power for nonlinear optical oscillation owing to the $1/Q^2$ scaling of the threshold[1].

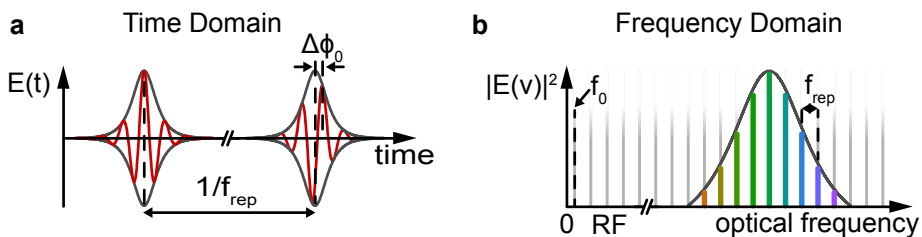


Figure 1.1: Time and frequency domain picture of mode-locked laser based frequency combs. A periodic train of pulses with a pulse repetition rate f_{rep} (panel a) corresponds to a comb spectrum of equidistant lines in the frequency domain (panel b). The line spacing is given by f_{rep} . The offset f_0 of the frequency comb spectrum relates to the carrier-envelope phase shift $\Delta\phi_0$ between two consecutive pulses via $f_0 = f_{\text{rep}} \cdot \Delta\phi_0 / (2\pi)$. The two parameters f_{rep} and f_0 fully define all comb frequencies $f_n = n \cdot f_{\text{rep}} + f_0$.

In 2007 it was discovered[13] that Kerr-nonlinear optical microresonators can give rise to optical frequency comb[14, 15] generation. The surprising cascade and mode proliferation associated with four-wave mixing (FWM) was demonstrated to lead to a broadband series of optical lines equidistantly spaced in the optical frequency domain, that is an optical frequency comb. The discovery of these so-called microresonator *Kerr-combs* established optical microresonators as tools for precision frequency metrology, a connection not made before. Such frequency comb spectra are conventionally derived from mode-locked femto-second lasers. In this way, Kerr-combs broke with the conventional dogma in the frequency metrology community, that an optical frequency comb requires a mode-locked pulsed laser source. Different from conventional mode-locked laser based combs, regular microresonator Kerr-combs are not pulsed in the time domain. By comparing the comb spectrum from a microresonator with a conventional mode-locked fiber laser comb, the equidistance of the comb lines could be proven at the level of 1 part in 10^{17} . Since this work the field of microresonator Kerr-combs has increased substantially. In the subsequent years, Kerr-combs have been demonstrated in a variety of platforms, including crystalline resonators[16], CMOS compatible platforms such as sili-

con nitride (Si_3N_4)[17, 18, 19], Hydrex glass[20], as well as aluminum nitride [21] or diamond[22]. In addition to allowing for miniaturization and chip-scale integration of frequency comb oscillators, microresonator based Kerr-combs enable to attain wide comb line spacings in the technologically relevant 10 – 100 GHz range[23, 24], which is not easily accessible using mode-locked laser frequency combs. Such large mode spacing is of particular interest in coherent telecommunication[25], spectrometer calibration for astronomy[26, 27], low noise microwave[28, 29] and arbitrary optical waveform generation[30]. Optical temporal dissipative cavity Kerr solitons, predicted theoretically[31, 32] and first realized experimentally in optical fibers[33], have played a decisive role in allowing to overcome noise processes associated with comb formation in microresonators. As detailed later, temporal *dissipative Kerr solitons* (DKS) provide a deterministic way to generate broadband, coherent, and spectrally smooth optical frequency combs, which are in addition amenable to an analytical theory and numerical simulation. These developments, along with the experimental generation of single soliton states in crystalline resonators[34, 35] and integrated Si_3N_4 resonators[36], make microresonators suitable for precision frequency metrology and many related applications. Owing to the pulsed nature of the solitons (in contrast to the earlier Kerr-combs), microresonators can now provide equivalent counterparts to mode-locked laser regarding the time domain properties. This allows using methods of spectral transfer and broadening as well as self-referencing techniques [37, 38, 39] that have been developed for mode locked laser-systems. In this way DKS in microresonators provide a route to synthesize absolute optical frequencies from an RF or microwave signal and the opportunity to use microresonators for counting the cycles of light.

1.2 Resonator platforms

Parametric frequency conversion in Kerr-nonlinear microresonators, first observed in toroidal fused silica and crystalline microresonators, has now been observed in a wide variety of geometries and platforms, including microspheres[40, 41] and integrated, planar ring-type resonators, such as those based on Si_3N_4 [42]. The work presented in this chapter on Kerr soliton generation has been carried out with crystalline magnesium fluoride MgF_2 resonators and Si_3N_4 integrated microrings, that are briefly described in the next sections.

1.2.1 Ultra high-Q MgF_2 Crystalline microresonators

The first microresonator platform in which temporal DKS have been observed experimentally[34] were crystalline resonators made from magnesium fluoride(MgF_2). Crystalline optical resonators were first introduced in [43] and further development demonstrated that polishing of crystalline materials can lead to exceptionally high Q-factors (exceeding 10^{11} [44, 45]). This method therefore extended the ultra high-Q attained with surface reflow methods[1, 46] to crystalline materials. Figure 1.2 shows an ultra high-Q crystalline resonator made from a MgF_2 cylindrical preform, which is prestructured with protrusions using precision diamond turning. After prestructuring a series of polishing steps using diamond films and slurries are used to attain a low roughness surface finish and ultra high-Q optical modes. To excite the whispering-gallery modes evanescent

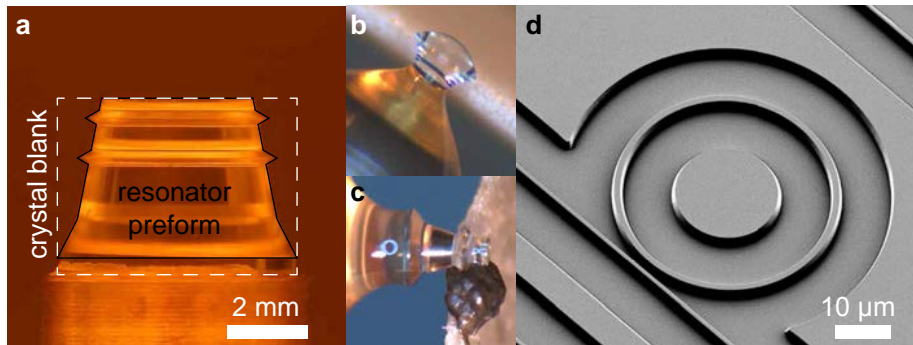


Figure 1.2: Microresonator platforms. (a) Diamond turned magnesium fluoride resonator containing two protrusions that confine high-Q optical whispering-gallery modes. (b) Manually shaped and polished resonator. (c) Polishing of a diamond turned preform. (d) Scanning electron micrograph of a silicon nitride microresonator before applying the fused silica cladding.

optical coupling via a tapered optical fiber can be used[47, 48]. This is possible as the refractive index of MgF_2 is lower than that of fused silica fibers. The use of thin tapered fiber for coupling is feasible despite the large volume of the employed (typically mm scale) resonators, due to the exceptionally high-Q, which reduces the necessary coupling rates required for critical coupling. Typically the resonance width is in the range from 50 – 500 kHz corresponding to Q values of 10^8 to several 10^9 . The nonlinear frequency conversion threshold is reached at optical powers below 1 mW. For soliton generation pump powers of the order of 10 mW are typical.

1.2.2 Integrated photonic chip microring resonators

From a future application perspective microresonator platforms amenable to wafer-scale processing can be advantageous. A key challenge in this context is attaining sufficiently high-Q for efficient nonlinear parametric frequency conversion. One platform that is particularly well suited is based on silicon nitride (Si_3N_4) waveguides embedded in fused silica. is a material already used in the micro-electronic industry (part of the CMOS process) and is well suited for integrated photonic waveguides. Its refractive index of $n \approx 2$ enables tight optical confinement waveguides and microring resonators and the high bandgap (~ 3 eV) mitigates two (or higher order) photon absorption in the telecommunication band. While the achieved Q-factors ($\sim 10^6$) in integrated devices are still many orders of magnitude below that of polished crystalline resonators, higher Kerr-nonlinearity and tighter optical confinement, lead to high effective nonlinearities that are almost three orders of magnitude larger than in crystalline resonators. This has enabled parametric oscillations to be accessible with pump powers of ~ 100 mW as demonstrated first in Refs. [18, 49]. Subsequent work demonstrated low phase noise comb operation[50] via nonlinear synchronization, as detailed later. In addition Si_3N_4 microresonators were the first microresonator platform that allowed for the observation of soliton induced

Cherenkov radiation[51] (or dispersive wave emission), i.e. the dynamics of solitons in the presence of higher order dispersion[52]. Fabrication of the resonators proceeds by lithography, etching and a final encapsulation technique in which the waveguides are clad with fused silica. The image of a final (but not yet clad resonator) is shown in Figure 1.2. Coupling to and from the chip is achieved with inverse tapered waveguides, adiabatically converting the mode spot diameter from a tight nanophotonic waveguide mode to a large area mode that can be excited with a lensed single-mode optical fiber.

1.3 Physics of the Kerr-comb formation process

In a simplified picture, the Kerr-comb formation in microresonators starts with an initial degenerate FWM process, generating a pair of sidebands symmetrically spaced in frequency around the pump laser in the resonances adjacent to the pumped resonance. In this process the free spectral range (FSR) defines the frequency spacing of the sidebands from the pump laser. A subsequent cascade of non-degenerate four-wave mixing processes generates a large series of sidebands in frequency steps corresponding to the initially defined line spacing. The bandwidth of the comb is limited by the dispersion of the resonator that causes a mismatch between the optical sidebands and the resonance frequencies. This mismatch increases with the spectral distance to the pump wavelength. While it explains well the early results of Kerr-frequency comb generation with typically THz-line spacing and moderate bandwidth, this picture had to be refined when attempting broader optical bandwidth and narrower line spacing (below 50 GHz) in toroidal [53], crystalline [16] and integrated Si_3N_4 resonators[17, 54, 55]. Here unexpected noise phenomena were observed in the form of broad optical lines, high amplitude noise and loss of coherence. These phenomena appeared to be independent of the chosen microresonator platform. Indeed, the origin of this noise can be explained by the universal properties of the comb formation mechanism[50]. While in early microresonator comb experiments, due to the wide line spacing, the mode proliferation occurred indeed on adjacent resonators modes, the latter is typically not the case in resonators with narrow FSR. Here the first pair of primary sidebands generated by the initial FWM process can occur in resonances that are widely separated from the pump (by multiple FSR). The process is depicted schematically in Figure 1.3. Using the nonlinear coupled mode equations, as introduced in the next section, one can show that the mode spacing between the primary modes is essentially defined by the (normalized) ratio of second order dispersion parameter and resonance width. If the resonator has a comparatively narrow FSR, then the initial sidebands are separated by a frequency interval Δ that encompasses a high number of FSR intervals. Further four-wave mixing can fill up the unpopulated resonances by formation of secondary sidebands separated by a smaller frequency spacing δ . In other words, sub combs with δ -line spacing form around the Δ -spaced primary lines. As, however, the primary spacing Δ is not guaranteed to be an integer multiple of the secondary spacing δ , the generated lines can not generally form a consistent comb, which manifests itself in the previously mentioned noise. This hypothesis of comb formation has been experimentally tested in [50] using a fiber laser frequency comb as a reference to reconstruct the frequency components of the Kerr-comb. Another key finding of this work

is that in contrast to the early model of comb formation, more than one single comb line can occupy a given resonance (cf. Figure 1.3 and Figure 1.4).

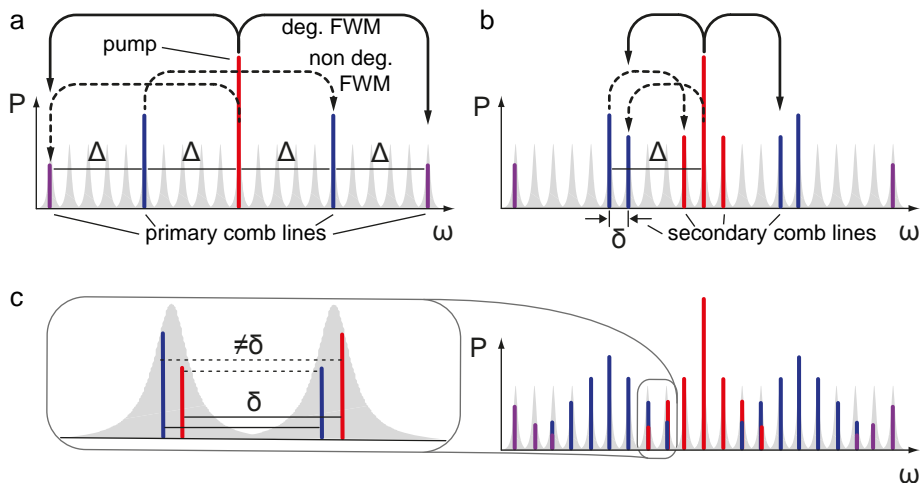


Figure 1.3: Universal Kerr-comb formation processes. (a) Formation of primary sidebands (b) Formation of subcombs (c) Overlap between inconsistent subcombs can lead to multiple lines per cavity resonance and explains noise phenomena in Kerr-combs.

Despite these noise processes, regimes have been found where broadband coherent Kerr-combs can be generated. The first observed transition to such a regime of low phase noise was presented in [50]. Here the subcombs defined by Δ and δ can be synchronized by changing the pump laser frequency and power so that Δ and δ become commensurate. Once close enough to the commensurate state, nonlinear synchronization and locking sets in and creates a phase coherent optical frequency comb [50] (albeit not pulsed in the time domain). Such synchronization has been experimentally observed and studied by reconstruction of the frequencies of the Kerr-comb lines as shown in Figure 1.5. Once the Kerr-comb falls into such a synchronized state it remains stable against fluctuations in the pump laser parameters and can be used for further experiments.

Later experiments have revealed that the nonlinear locking process can be captured by the Adler equation, that is known from injection locking of lasers [56]. Kerr combs driven into a low-phase noise, coherent state have been used in applications, such as coherent communications [25], where they are used to provide a multitude of data channels from a single laser, enabling terabit per second data-communication. Yet, despite the promising prospects a central missing element has been ways to reliably achieve such low phase noise combs, with smooth spectral envelope. A surprising discovery has been made in 2012 [57, 34], when it was demonstrated that the generated subcombs can not only undergo nonlinear synchronization, but moreover can seed the formation of temporal DKS in optical microresonators. This discovery provides not only an opportunity to study DKS in microresonators, but moreover a powerful tool to generate low phase noise combs with broad spectral bandwidth that can be used in a variety of applications. Before turning to soliton formation, we review first

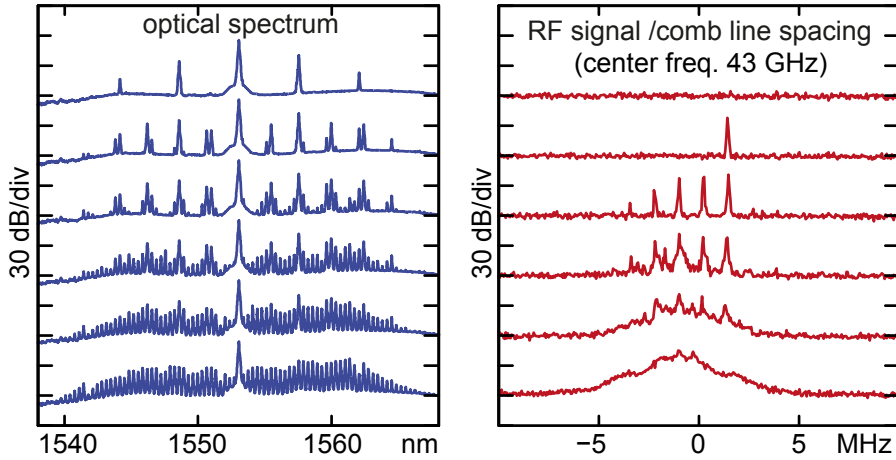


Figure 1.4: Kerr-comb formation and noise. (a) Formation of the optical spectrum as the laser is tuned into resonance and the intracavity power increases. (b) Comb-line spacing measured as the radio-frequency (RF) beatnote between neighboring comb lines. Multiple and broad beatnotes indicate multiple and inconsistent line spacings present in the comb spectrum.

the basic formalism describing Kerr-nonlinearity driven parametric oscillations.

1.3.1 Nonlinear coupled mode equations

The theoretical analysis of parametric oscillations, frequency comb and soliton formation is a complex nonlinear mathematical problem for which several approaches have been proposed [11, 58, 41, 59, 60, 61]. Besides description in the time domain the modal expansion approach in the frequency domain [62, 63] has proven particularly useful in the context of microresonators as it allows easily to take into account particularities in the mode structure. The system of equations describing the dynamics of each optical mode A_m in the slowly varying envelope approximation can be obtained from the nonlinear wave equation in conjunction with the quantum Langevin equations:

$$\begin{aligned}
\frac{\partial A_m}{\partial t} &= -\frac{\kappa_m}{2} A_m + \delta_{m,m_0} \sqrt{\frac{\kappa_{\text{ex},m} P_{\text{in}}}{\hbar \omega_0}} e^{-i(\omega_p - \omega_0)t} \\
&+ ig \cdot \sum_{m',m'',m'''} \Lambda_m^{m'm''m'''} \mathcal{D}_m^{m'm''} A_{m'} A_{m''} A_{m'''}^* e^{-i(\omega'_m + \omega''_m - \omega'''_m - \omega_m)t} \\
&+ \sqrt{\kappa_{\text{i},m}} \delta s_{\text{i},m}(t) + \sqrt{\kappa_{\text{ex},m}} \delta s_{\text{ex},m}(t).
\end{aligned} \tag{1.1}$$

Here κ_m denotes the cavity decay rate of mode m with eigenfrequency ω_m , \hbar is the reduced Planck constant. The cavity decay rate is composed of intrinsic ($\kappa_{\text{i},m}$) and external coupling ($\kappa_{\text{ex},m}$) loss rates such that the total loss rate is $\kappa_m = \kappa_{\text{i},m} + \kappa_{\text{ex},m} = \frac{\omega_m}{Q_m}$, where Q_m is the loaded quality-factor of mode m . One mode (m_0, ω_0) is driven by a classical field with optical power P_{in} and frequency ω_p . The terms $\delta s_{\text{i},m}$ and $\delta s_{\text{ex},m}$ designate quantum Langevin input noises with commutation relations $[\delta s_j(t), \delta s_j^\dagger(t')] = \delta(t - t')$ and with zero

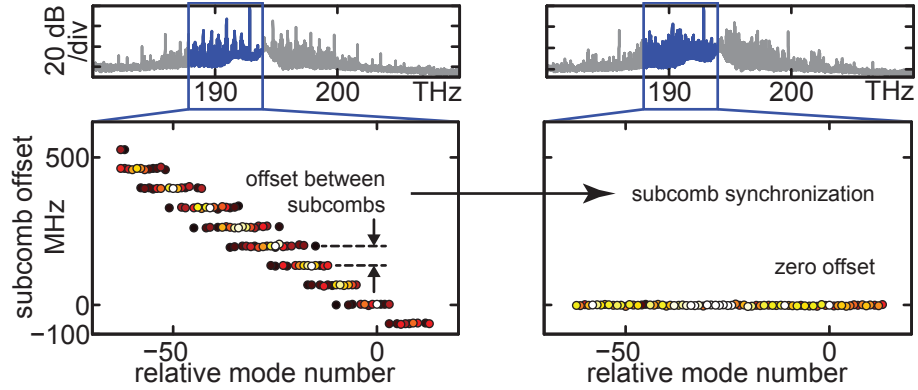


Figure 1.5: Subcomb synchronization in a Si_3N_4 optical microresonator achieved by changing the pump laser wavelength..

mean ($\langle \delta s_j(t) \rangle = 0$). The summation over the nonlinear interaction terms is made over all azimuthal indices for the nearly equidistant set of fundamental whispering-gallery eigenmodes, satisfying the following conservation relation: $m' + m'' - m''' = m$, where $\mathcal{D}_m^{m' m''}$ is the degeneracy factor: $\mathcal{D}_m^{m' \neq m''} = 2$ in case of cross-phase modulation and non-degenerate four-wave mixing, and $\mathcal{D}_m^{m' m''} = 1$ for self-phase modulation and hyperparametric generation. We neglect processes where one of the frequencies is significantly smaller ($\omega_m = \omega_{m'} - \omega_{m''} - \omega_{m'''}$) or larger than other frequencies ($\omega_m = \omega_{m'} + \omega_{m''} + \omega_{m'''}$) as it is the case for third harmonic generation (when in the degenerate case $\mathcal{D}_{3m'}^{m' m' m'} = 1/3$). The intermodal coupling factor is given by

$$\Lambda_m^{m' m'' m'''} = \frac{\int \mathbf{e}_{m'} \mathbf{e}_{m''} \mathbf{e}_{m'''}^* \mathbf{e}_m dV}{\int |\mathbf{e}_0|^4 dV} \frac{\chi^{(3)}(\omega_m = \omega_{m'} + \omega_{m''} - \omega_{m'''})}{\chi^{(3)}(\omega_0 = \omega_0 + \omega_0 - \omega_0)}, \quad (1.2)$$

where \mathbf{e}_m is vector electric field distribution of the mode m and $\chi^{(3)}$ describes the third order Kerr-nonlinearity. This factor is analytically different from that obtained in [61, 62, 63]¹. The effective nonlinear volume of the modes is given by:

$$V_m = \frac{(\int |\mathbf{e}_m|^2 dV)^2}{\int |\mathbf{e}_m|^4 dV}. \quad (1.3)$$

The latter may be found from the cavity eigenmodes' field distribution. The modes are normalized such that $|A_m|^2$ corresponds to the number of photons in a given cavity mode. The nonlinear coupling constant g (that is the Kerr frequency shift per photon) is defined as in [58]:

$$g = \frac{3\hbar\omega_0^2 \chi^{(3)}(\omega_0)}{4\epsilon_0 n^4(\omega_0) V_0} = \frac{\hbar\omega_0^2 c n_2(\omega_0)}{n^2(\omega_0) V_0}. \quad (1.4)$$

¹The authors of [61, 62, 63] overlooked in the derivation that the nonlinear polarization is time dependent and can not be simply taken out from the time derivative in wave equation [64]. This omission leads to unphysical asymmetry in Λ over mode indices and loss of precise degeneracies important for analytical considerations, but usually plays negligible role in numerical simulations of narrow combs when $\Lambda \simeq 1$.

Here ϵ_0 denotes the dielectric constant and n and n_2 are the refractive non-linear optical indices. A seeding via input noises is important for numerical simulations to initiate the comb, however, it is not required in further analytical considerations as their means vanish.

For the calculation of the field distribution and eigenfrequencies in crystalline resonators we do not use the modes of a sphere as proposed in [62, 63] but asymptotic solutions obtained for a spheroid [65, 66, 67], producing better approximations for the wide range of geometries, or eigenfrequencies obtained via COMSOL finite element modeling. From these approximations as well as from Sellmeier's equation for the resonator material one can determine V_m and eigenfrequencies ω_m to find second and higher order dispersions. The latter allows can be approximated by

$$\omega_\mu \approx \omega_0 + D_1\mu + \frac{1}{2!}D_2\mu^2 + \frac{1}{3!}D_3\mu^3, \quad (1.5)$$

where $\mu = m - m_0$. The parameter D_2 is related to the second order group velocity dispersion (GVD) β_2 ($\beta_j = \frac{\partial^j \beta}{\partial \omega^j}$) via $D_2 = -\frac{c}{n}D_1^2\beta_2$, and D_3 relates to the third order dispersion via $D_3 = -\frac{c}{n}D_1^3\beta_3 + 3\frac{c^2}{n^2}D_1^3\beta_2^2 \approx -\frac{c}{n}D_1^3\beta_3$.

It is convenient to remove the explicit time dependence in the nonlinear equations with the substitution $A_\mu = \tilde{A}_\mu e^{i(\omega_\mu - \omega_p - \mu D_1)t}$, where $D_1/(2\pi)$ is the mode spacing of the comb at the pump wavelength. Moreover, the pump term is written as $F = \sqrt{\frac{\kappa_e P_{in}}{\hbar \omega_0}}$. In this new basis the oscillations of each optical mode are considered not around eigenfrequencies but around nearest frequencies on an equidistant D_1 spaced-grid:

$$\begin{aligned} \frac{\partial \tilde{A}_\mu}{\partial t} = & - [i(\omega_\mu - D_1\mu - \omega_p) + \frac{\kappa_\mu}{2}] \tilde{A}_\mu + \delta_{\mu 0} F \\ & + ig \sum_{\mu', \mu'', \mu'''} \Lambda_\mu^{\mu' \mu'' \mu'''} \tilde{A}_{\mu'} \tilde{A}_{\mu''} \tilde{A}_{\mu' + \mu'' - \mu}^*. \end{aligned} \quad (1.6)$$

If L pairs of sidebands and the pump are considered, then the total number of nonlinear terms in all $2L + 1$ equations is $\frac{1}{3}(L + 1)(8L^2 + 7L + 3)$.

It is possible to get some useful conservation laws for this set of equations. Calculating the evolution of the total number of photons in the comb $\frac{dN}{dt} = \sum_{\mu=-L}^L \frac{dN_\mu}{dt}$, with $\frac{dN_\mu}{dt} = \frac{dA_\mu}{dt} A_\mu^* + \frac{dA_\mu^*}{dt} A_\mu$ and assuming symmetry: $\Lambda_\mu^{\mu' \mu'' \mu'''} + \Lambda_{\mu'''}^{\mu'' \mu' \mu} = \Lambda_{\mu'}^{\mu'' \mu'''} + \Lambda_{\mu''}^{\mu'''} \mu'$, we find that most of the terms in the sum cancel each other:

$$\frac{dN}{dt} + \sum_{\mu=-L}^L \kappa_\mu N_\mu = (FA_0^* + F^*A_0), \quad (1.7)$$

which in case of $\kappa_\mu = \kappa$ simplifies to

$$\frac{dN}{dt} + \kappa N = 2|F||A_0| \cos \phi_0, \quad (1.8)$$

where ϕ_0 is the phase difference between F and A_0 . This master equation for the whole optical spectrum may be useful for example for the analysis of the steady states.

In a similar way one may find:

$$\sum_{\mu=-L}^L \mu \left(\frac{dN_{+\mu}}{dt} - \frac{dN_{-\mu}}{dt} \right) = - \sum_{\mu=-L}^L \mu (\kappa_{+\mu} N_{+\mu} - \kappa_{-\mu} N_{-\mu}), \quad (1.9)$$

which in the case of steady state means that the 'center of mass' (i.e. the frequency center of photonic energy) of the spectrum is conserved and coincides with the pump frequency as each four-wave mixing process follows this conservation law.

In the following analysis we use further simplifications, assuming equal parameters for all comb lines ($\kappa_m = \kappa$, $\Lambda_m^{m'm''m'''} = 1$) and renumbering comb lines with index μ , starting from the central driven mode m_0 , i.e. $\mu = m - m_0$. In this case it is possible to write the equations in a dimensionless way, as suggested in [58]:

$$\begin{aligned} a_\mu &= \tilde{A}_\mu \sqrt{2g/\kappa}, \\ f &= \sqrt{8g/\kappa^3} |F_p|, \\ \zeta_\mu &= 2(\omega_\mu - \mu D_1 - \omega_p)/\kappa \approx \zeta_0 + D_2 \mu^2/\kappa, \\ \tau &= \kappa t/2, \end{aligned} \quad (1.10)$$

$$\frac{\partial a_\mu}{\partial \tau} = -[1 + i\zeta_\mu]a_\mu + i \sum_{\mu', \mu''} a_{\mu'} a_{\mu''} a_{\mu'+\mu''-\mu}^* + \delta_{0\mu} f. \quad (1.11)$$

In this form all frequencies, detunings and magnitudes are measured in units of cavity resonance width so that $|a_\mu|^2 = 1$ corresponds to the nonlinear mode pulling of one cavity resonance width (thresholds for both single mode bistability and degenerate oscillations).

1.3.2 Degenerate hyperparametric oscillations

An analytic solution of the complete nonlinear system with many comb lines in general case is hardly possible. It is possible, however, to resolve equations for an arbitrary set of modes if only degenerate processes caused by the pump as well as nonlinear mode pulling effects corresponding to cross- and self-phase modulation are taken into account. These effects are dominating as long as the energy in each of the optical lines is small compared to the intracavity pump power and when due to strong second order dispersion the resonator modes are far enough from equidistance lines to suppress non-degenerate four-wave mixing.

The following set of reduced equations qualitatively describes the processes of initial comb formation, including widely spaced primary lines, switching between initially excited modes, chaotic behavior and noisy RF signals with many frequencies:

$$\begin{aligned} \frac{\partial a_0}{\partial \tau} &= -[1 + i\zeta_0]a_0 + i(2\tilde{N} - |a_0|^2)a_0 + 2i \sum_{\mu=1}^L a_\mu a_{-\mu} a_0^* + f, \\ \frac{\partial a_\mu}{\partial \tau} &= -[1 + i\zeta_\mu]a_\mu + i(2\tilde{N} - |a_\mu|^2)a_\mu + i a_{-\mu}^* a_0^2, \end{aligned} \quad (1.12)$$

where according to the normalization $\tilde{N} = 2gN/\kappa$. The reduced model was compared with the full numeric model integrated using the Runge-Kutta scheme.

It shows good agreement concerning the initially generated sidebands and qualitative agreement of the comb in the noisy, chaotic regime.

With the substitution $a_\mu = \alpha_\mu e^{-i\phi_\mu}$, $\psi_\mu = 2\phi_0 - \phi_\mu - \phi_{-\mu}$ it is possible to search for steady state solutions with $\dot{\alpha}_\mu = 0$ and $\dot{\phi}_\mu \equiv \delta\tilde{\omega}_\mu = \text{const}$. One may obtain a steady state from the resulting equations when $\dot{\phi}_0 = 0$ and $\dot{\psi}_\mu = 0$, so that $\dot{\phi}_\mu = -\dot{\phi}_{-\mu}$ and $\delta\tilde{\omega}_\mu = -\delta\tilde{\omega}_{-\mu} = D_3\mu^3/(3\kappa) + \dots$. Splitting the equations (1.12) into real and imaginary parts we get:

$$\begin{aligned} \alpha_0(1 + 2 \sum_{\mu=1}^L \alpha_\mu \alpha_{-\mu} \sin \psi_\mu) &= f \cos \phi_0, \\ (\zeta_0 - 2\tilde{N} - 2 \sum_{\mu=1}^L \alpha_\mu \alpha_{-\mu} \cos \psi_\mu + \alpha_0^2) \alpha_0 &= f \sin \phi_0, \\ \alpha_{\pm\mu} - \alpha_{\mp\mu} \alpha_0^2 \sin \psi_\mu &= 0, \\ \tilde{\zeta}_\mu \alpha_\mu - (2\tilde{N} - \alpha_\mu^2) \alpha_\mu - \alpha_{-\mu} \alpha_0^2 \cos \psi_\mu &= 0, \end{aligned} \quad (1.13)$$

where

$$\tilde{\zeta}_\mu = (\zeta_\mu - 2\dot{\phi}_\mu/\kappa). \quad (1.14)$$

From the third equation we find that $\alpha_\mu = \alpha_{-\mu}$ and $\psi_\mu \equiv \psi = \arcsin(1/\alpha_0^2)$. Substituting this into the first and second equation of (1.13) we obtain:

$$\begin{aligned} \tilde{N} &= f \alpha_0 \cos \phi_0, \\ [\zeta_0 - 2\tilde{N} + \alpha_0^2 + (\tilde{N} - \alpha_0) \sqrt{1 - 1/\alpha_0^4}] \alpha_0 &= f \sin \phi_0. \end{aligned} \quad (1.15)$$

The first equation of (1.15) also follows from the master equation (1.8). Adding both equations squared we get the system:

$$\begin{aligned} [\zeta_0 - \tilde{N}(2 + \cos \psi) + \alpha_0^2(1 + \cos \psi)]^2 \alpha_0^2 + \tilde{N}^2/\alpha_0^2 &= f^2, \\ \tilde{\zeta}_\mu + \alpha_\mu^2 - 2\tilde{N} = \tilde{\zeta}_{nl} = \alpha_0^2 \cos \psi. \end{aligned} \quad (1.16)$$

It follows that $\tilde{\zeta}_{nl}$, which determines the detuning of the new nonlinear effective eigenfrequency from the frequency of oscillations, does not depend on μ . This means that in the steady state an equidistant comb may be formed if the dispersion of each mode is compensated by nonlinear pulling with appropriate amplitude distribution of each excited comb line. This nonlinear dispersion compensation is possible due to the fact that self phase modulation is two times smaller than cross phase modulation and is an essential mechanism for comb formation [40, 68].

The last equations of (1.16) may be summed over all excited lines to get:

$$\tilde{N} = \frac{\zeta_\Sigma - \alpha_0^2 + 2L\sqrt{\alpha_0^4 - 1}}{4L - 1}, \quad (1.17)$$

where $\zeta_\Sigma = \sum_{\mu=-L}^L \tilde{\zeta}_\mu = (2L + 1)\zeta_0 + d_2 \sum_{\mu} \mu^2$ (where $d_2 = D_2/\kappa$). If excited comb lines are filling all resonator modes in some interval without omissions the summation may be done analytically. If substituted in the first equation of (1.16) we finally can get an equation for the pump mode magnitude α_0^2 ready

for numerical analysis. Substituting $\beta = \alpha_0^2 - \sqrt{\alpha_0^4 - 1}$, $\alpha_0^2 = \frac{\beta^2 + 1}{2\beta}$ then transforms the final equation to a rational 6-th order equation. Further analysis of these equations may reveal the properties of the low-noise low-populated combs observable in experiments.

1.3.3 Primary sidebands

A particular case of the reduced model is a three mode system for which all the nonlinear terms are in fact considered, i.e. the model is complete. This system can describe the threshold for primary sideband hyperparametric oscillations at a μ times FSR frequency separation from the pump that can be softly excited when the pump is gradually tuned into resonance starting from infinite detuning ($\omega_0 < \omega_p$ for $D_2 > 0$).

The three mode system and its stability was analyzed in detail using numerical analysis of the nonlinear equations [58] or stability analysis of the linearized equations [62]. Both approaches lead to the same equation following from the reduced model when $L = 1$:

From the nonlinear resonance condition and condition for the first sideband to emerge ($\alpha_{\mu,\text{th}}^2 = 0, \tilde{N} = \alpha_0^2$) we obtain:

$$\begin{aligned} (\zeta_0 - \alpha_0^2)^2 \alpha_0^2 + \alpha_0^2 &= f^2, \\ \zeta_0 + d_2 \mu^2 &= 2\alpha_0^2 - \sqrt{\alpha_0^4 - 1}. \end{aligned} \quad (1.18)$$

It follows the equation determining the possibility to excite the mode μ :

$$\begin{aligned} \zeta_0 &= \alpha_0^2 - \sqrt{f^2/\alpha_0^2 - 1}, \\ \sqrt{f^2/\alpha_0^2 - 1} - d_2 \mu_{\text{th}}^2 + \alpha_0^2 - \sqrt{\alpha_0^4 - 1} &= 0. \end{aligned} \quad (1.19)$$

or using the smallest possible $\alpha_0^2 = 1$ when the radical is real:

$$\mu_{\text{th}} = \left\lfloor \sqrt{(1 + \sqrt{f^2 - 1})/d_2} \right\rfloor. \quad (1.20)$$

Alternatively, this can be rewritten in physical terms [50] as:

$$\mu_{\text{th}} = \left\lfloor \sqrt{\frac{\kappa}{D_2} (1 + \sqrt{\frac{P_{\text{in}}}{P_{\text{th}}} - 1})} \right\rfloor. \quad (1.21)$$

The threshold power P_{th} corresponds to $|a_{0,\text{th}}| = 1$. The minimum obtainable μ_{th} for $P_{\text{in}} = P_{\text{th}}$ is given by:

$$\mu_{\text{th}} = \sqrt{\frac{D_2}{\kappa}}, \quad (1.22)$$

and depends only on the ratio of cavity decay rate κ to second order cavity dispersion D_2 .

Note that the threshold $\alpha_{0,\text{th}} = 1$, determining the first sideband to appear when tuning the pump into resonance at a given power (also found in [62]), however, does not correspond to a minimum of input power when hyperparametric generation may start. This minimum, numerically calculated in [58] may be found explicitly as $\alpha_{\text{in},\text{min}} = 2/\sqrt{3}$.

1.4 Dissipative Kerr solitons in optical microresonators

The formation of stable temporal DKS circulating in a continuous-wave (CW) driven microresonator with Kerr-nonlinearity is a remarkable form of optical self-organization. It requires, similarly to the Kerr-combs described above, a medium with focusing third order nonlinearity and anomalous group velocity dispersion. Fundamentally different from the above described Kerr-combs, the formation of temporal DKS implies a stable pulsed time domain waveform where the pulse properties are fully determined by the experimental parameters. The ultra-short soliton pulse duration, typically in the femto-second regime, implies broadband optical frequency comb spectra that show the same wide line spacing that is known from the previous Kerr-combs. Importantly, however, the soliton based comb spectra do not suffer from the inconsistent subcomb formation and associated noise processes that are often observed in Kerr-combs. Prior to the observation in a microresonator, temporal DKS had already been observed in a several hundred meter long, CW driven fiber cavity, where additional short laser pulses had been used to stimulate the soliton formation [33]. In this context it was speculated that DKS could be formed in a microresonator as well (Note: the possibility of solitons circulating in a dielectric sphere was already proposed in Ref. [69]). Moreover, Refs. [70, 71] pointed out that the theoretical formalism so far used by researchers to describe microresonators and fiber-cavities, i.e. the non-linear coupled mode equations and the Lugiato-Lefever equation [72] respectively, can be mapped onto each other. From a historical perspective, it is thus interesting to note that after the first reports on microresonator Kerr-combs in 2007[13], it took five years to enter the regime of Kerr solitons in a microresonator. One reason for this is the particular thermal behavior of a microresonator system that had long masked this regime (cf. Section 1.6). Moreover, the approach of stimulating solitons using laser pulses that is successfully used with long fiber cavities can not easily be transferred to microresonators due to their much higher finesse (i.e. difficulty of coupling the pulse to into the resonator). Before presenting experimental observations, the following section will establish the theoretical formalism that allows describing dissipative Kerr soliton in a microresonator.

1.4.1 Analytical theory of dissipative Kerr solitons

To describe the internal field in a nonlinear microresonator the following master equation may be used when third and higher order dispersion terms are neglected [60, 70]:

$$\frac{\partial A}{\partial t} - i\frac{1}{2}D_2\frac{\partial^2 A}{\partial \phi^2} - ig|A|^2A = -\left(\frac{\kappa}{2} + i(\omega_0 - \omega_p)\right)A + \sqrt{\frac{\kappa\eta P_{\text{in}}}{\hbar\omega_0}}. \quad (1.23)$$

Here $A(\phi, t) = \sum_{\mu} A_{\mu} e^{i\mu\phi - i(\omega_{\mu} - \omega_p)t}$ is the slowly varying field amplitude and $\phi \in [0, 2\pi]$ is the angular coordinate inside the resonator with periodic boundary conditions, $\eta = \kappa_{ex}/\kappa$ is the coupling efficiency with critical coupling corresponding to $\eta = 1/2$. Transforming eq. (1.23) to its dimensionless form gives:

$$i\frac{\partial \Psi}{\partial \tau} + \frac{1}{2}\frac{\partial^2 \Psi}{\partial \theta^2} + |\Psi|^2\Psi = (-i + \zeta_0)\Psi + if. \quad (1.24)$$

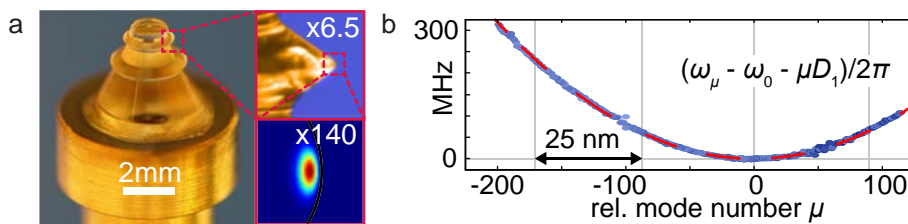


Figure 1.6: Crystalline resonator for dissipative Kerr soliton generation. (a) Crystalline MgF_2 resonator and simulated mode profile. (b) Measured anomalous group velocity dispersion for the resonator shown in panel a. The dispersion of a resonator can be quantified in terms of the deviation of its resonance frequencies ω_μ from an equidistant frequency grid $\omega_0 + \mu D_1$, where $D_1/(2\pi)$ is the FSR at the pump wavelength. An anomalous group velocity dispersion corresponds to a parabolic curve as shown in panel b.

Here $\Psi(\tau, \phi) = \sum a_\mu(\tau) e^{i\mu\phi}$ is the waveform, $\theta = \phi \sqrt{\frac{1}{2d_2}}$ is the dimensionless longitudinal coordinate, and $d_2 = D_2/\kappa$ is the dimensionless dispersion. Equation (1.24) is identical to the Lugiato-Lefever equation [72], where a transversal coordinate is used instead of a longitudinal one in our case. It is important to note here, that though we used throughout the chapter the term *temporal* to differentiate DCS from better known spacial cavity solitons in nonlinear Fabry-Perot etalons, this term may also be confusing. For temporal dissipative solitons in fibers and fiber loop resonators in equations time is usually considered as a “fast” variable, describing the form of the pulse, while the coordinate along propagation is describing slow variations. In the case of WGM microresonators the opposite mapping is more convenient with “slow” time variation averaged over many roundtrips and fast mapped azimuthal angular coordinate. The equation 1.24 may also be considered as a driven, damped Nonlinear Schrödinger Equation (NLS) [31]. Analytical solution of the NLS in the form of bright soliton is known only in case of zero dissipation [73]. An approximate solution for the dissipative soliton may be found using Lagrangian perturbation approach [74, 75]. First we introduce Lagrangian density so that the variation of it over Ψ^* (Landau-Euler equation) leads to an unperturbed NLS equation:

$$\frac{\delta \mathcal{L}}{\delta \Psi^*} \equiv \frac{\partial \mathcal{L}}{\partial \Psi^*} - \frac{\partial}{\partial \tau} \frac{\partial \mathcal{L}}{\partial \Psi_\tau^*} - \frac{\partial}{\partial \theta} \frac{\partial \mathcal{L}}{\partial \Psi_\theta^*} = 0, \quad (1.25)$$

$$\mathcal{L} = \frac{i}{2} \left(\Psi^* \frac{\partial \Psi}{\partial \tau} - \Psi \frac{\partial \Psi^*}{\partial \tau} \right) - \frac{1}{2} \left| \frac{\partial \Psi}{\partial \theta} \right|^2 + \frac{1}{2} |\Psi|^4 - \zeta_0 |\Psi|^2. \quad (1.26)$$

Now taking into account the perturbed equation (1.24) we introduce the dissipative function:

$$\begin{aligned} \frac{\delta \mathcal{L}}{\delta \Psi^*} &= \mathcal{R}, \\ \mathcal{R} &= -i\Psi + if. \end{aligned} \quad (1.27)$$

The equations that need to be solved are the following:

$$\begin{aligned} \frac{\partial L}{\partial r_i} - \frac{d}{d\tau} \frac{\partial L}{\partial \dot{r}_i} &= \int \left(\mathcal{R} \frac{\partial \Psi^*}{\partial r_i} + \mathcal{R}^* \frac{\partial \Psi}{\partial r_i} \right) d\theta, \\ L &= \int \mathcal{L} d\theta. \end{aligned} \quad (1.28)$$

where r_i are different possibly time dependent collective coordinates. Using the ansatz of a stationary ($\frac{\partial \Psi}{\partial \tau} = 0$) soliton $Be^{i\varphi_0} \text{sech}(B\theta)$ (exact for unperturbed case when $B = \sqrt{2\zeta_0}$) with $r_1 = B$ and $r_2 = \varphi_0$ [32] we get:

$$L = -2B \frac{\partial \phi_0}{\partial \tau} + \frac{1}{3} B^3 - 2B\zeta_0. \quad (1.29)$$

This yields:

$$\frac{dB}{d\tau} = -2B + \pi f \cos \varphi_0, \quad (1.30)$$

$$\frac{d\phi_0}{d\tau} = \frac{1}{2} B^2 - \xi_0. \quad (1.31)$$

This leads to the stationary parameters of the soliton attractor [32]:

$$B = \sqrt{2\zeta_0}, \quad (1.32)$$

$$\cos \varphi_0 = \frac{2B}{\pi f} = \frac{\sqrt{8\zeta_0}}{\pi f}, \quad (1.33)$$

$$\zeta_0^{\max} = \frac{\pi^2 f^2}{8}. \quad (1.34)$$

An approximate single soliton solution which accounts for a flat CW background is then given by

$$\Psi = \Psi_0 + \Psi_1 \simeq \Psi_0 + Be^{i\varphi_0} \text{sech}(B\theta), \quad (1.35)$$

The constant CW background Ψ_0 may be found by inserting Ψ_0 into eq. (1.24) as the lowest branch [31] of the solution of

$$(|\Psi_0|^2 - \zeta_0 + i)\Psi_0 = if, \quad (1.36)$$

which, eventually, results for $\zeta_0 > \sqrt{3}$ (bistability criterion) and large enough detunings $f^2 < \frac{2}{27}\zeta_0(\zeta_0^2 + 9)$ in:

$$\begin{aligned} |\Psi_0|^2 &= \frac{2}{3}\zeta_0 - \frac{2}{3}\sqrt{\zeta_0^2 - 3} \cosh\left(\frac{1}{3} \text{arcosh}\left(\frac{2\zeta_0^2 + 18\zeta_0 - 27f^2}{2(\zeta_0^2 - 3)^{2/3}}\right)\right), \\ \Psi_0 &= \frac{if}{|\Psi_0|^2 - \zeta_0 + i} \simeq \frac{f}{\zeta_0^2} - i\frac{f}{\zeta_0}. \end{aligned} \quad (1.37)$$

Extending (1.35) to the case of multiple solitons inside the resonator gives

$$\Psi(\phi) \simeq \Psi_0 + \left(\frac{4\zeta_0}{\pi f} + i\sqrt{2\zeta_0 - \frac{16\zeta_0^2}{\pi^2 f^2}} \right) \sum_{j=1}^K \text{sech}\left(\sqrt{\frac{\zeta_0}{d_2}}(\phi - \phi_j)\right). \quad (1.38)$$

This ansatz automatically translates to discrete possible states (steps) in nonlinear resonant response. These steps are an important signature of soliton Kerr

combs and are observed in the experiments (see below). The height of steps in the intracavity power can be found by averaging the waveform amplitude (eq. 1.38) squared over one roundtrip for different numbers K of solitons:

$$\begin{aligned} |\overline{\Psi}|^2 &= |\Psi_0|^2 + K \frac{1}{2\pi} \int_0^{2\pi} (\Psi_1^2 + \Psi_0 \Psi_1^* + \Psi_1 \Psi_0^*) d\phi \\ &\simeq \frac{f^2}{\zeta_0^2} + K \frac{2}{\pi} \sqrt{d_2 \zeta_0}. \end{aligned} \quad (1.39)$$

The Fourier transform (\mathcal{F}) of a hyperbolic secant soliton is again a hyperbolic secant:

$$\Psi(\mu) = \mathcal{F} \left[\sqrt{2\zeta_0} \operatorname{sech} \left(\sqrt{\frac{\zeta_0}{d_2}} \phi \right) \right] = \sqrt{d_2/2} \operatorname{sech} \left(\frac{\pi\mu}{2} \sqrt{\frac{d_2}{\zeta_0}} \right). \quad (1.40)$$

Using the relation for the optical frequency $\omega = \omega_p + \mu D_1$ and the time $t = \phi/D_1$ the spectral envelopes and the soliton waveform can be rewritten:

$$\Psi(\omega - \omega_p) = \sqrt{d_2/2} \operatorname{sech}((\omega - \omega_p)/\Delta\omega) \quad \text{with} \quad \Delta\omega = \frac{2D_1}{\pi} \sqrt{\frac{\zeta_0}{d_2}}, \quad (1.41)$$

and

$$\Psi(t) = \sqrt{2\zeta_0} \operatorname{sech}(t/\Delta t), \quad \text{with} \quad \Delta t = \frac{1}{D_1} \sqrt{\frac{d_2}{\zeta_0}}. \quad (1.42)$$

The minimal possible soliton duration can be found by using ζ_0^{\max} (eq. 1.33) in the above equation for Δt :

$$\Delta t_{\min} = \frac{1}{\pi D_1} \sqrt{\frac{\kappa D_2 n_0^2 V_{\text{eff}}}{\eta P_{\text{in}} \omega_0 c n_2}}. \quad (1.43)$$

This equation can be recast in form of the group velocity dispersion $\beta_2 = \frac{-n_0}{c} D_2/D_1^2$, the nonlinear parameter $\gamma = \frac{\omega}{c} \frac{n_2}{\mathcal{A}_{\text{eff}}}$ (for simplicity we assume critical coupling $\eta = 1/2$ and on resonant pumping):

$$\Delta t_{\min} = \frac{2}{\sqrt{\pi}} \sqrt{\frac{-\beta_2}{\gamma \mathcal{F} \mathcal{P}_{\text{in}}}}, \quad (1.44)$$

where denotes the finesse $\mathcal{F} = \frac{D_1}{\kappa}$ of the cavity. Note that the values $\Delta\omega$ and Δt need to be multiplied by a factor of $2 \operatorname{arccosh}(\sqrt{2}) = 1.763$ to yield the FWHM of the sech^2 -shaped power spectrum and pulse intensity, respectively.

For the time bandwidth product (TBP) we find $\Delta t \cdot \Delta\omega = 2/\pi$ or, when considering the FWHM of spectral and temporal power (in units of Hz and s), $\text{TBP} = 0.315$.

In the case of K multiple solitons inside the cavity there is a more structured optical spectrum Ψ_k , resulting from interference of single soliton spectra $\Psi_j(\mu)$, where the relative phases of these spectra are determined by the positions ϕ_j of individual solitons: $\Psi_K(\mu) = \Psi(\mu) \sum_{j=1}^K e^{i\mu\phi_j}$. The line-to-line variations can be high, however, the overall averaged spectrum still follows the single soliton shape and is proportional to $\sqrt{K} \Psi(\mu)$.

1.5 Signatures of dissipative Kerr soliton formation in crystalline resonators

The generation of DKS in microresonators is associated with several characteristic signatures that can already be observed during a transient generation of the solitons. Here transient generation refers to the situation where the pump laser is scanned (with increasing wavelength) through the resonance of the microresonator. The described signatures are particularly useful from a practical perspective as they allow for rapid sample characterization. Depending on the detuning during the laser scan the system can enter different nonlinear regimes including, parametric sideband generation with Turing patterns[76], Kerr-comb formation, breather solitons [77] and stable dissipative Kerr soliton generation. One signature, though not unambiguously connected to soliton formation, is a transition from high intensity noise and high phase noise (related to Kerr-subcomb formation) to a low noise state. While scanning the laser, the noise can be monitored by e.g. recording the intensity noise in the generated spectrum or by detecting the beatnote signal between the generated optical lines as shown in Figure 1.7b.

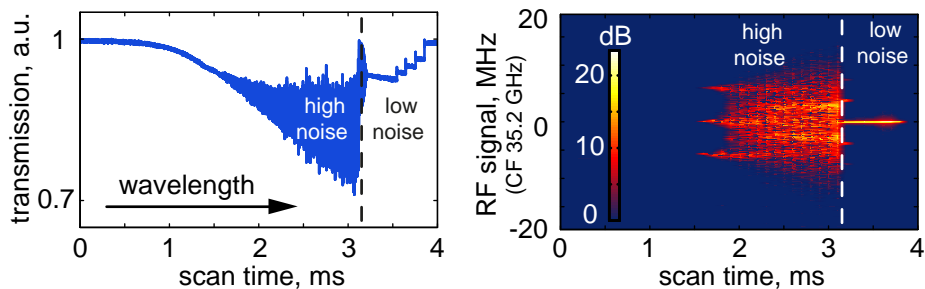


Figure 1.7: Signatures of soliton formation. (a) A staircase-like step structure in the pump laser transmission indicates the formation of several temporal DKS in the microresonator. High intensity noise is apparent in the transmission signal prior to soliton formation. (b) The formation of the solitons is associated with a transition to low noise. This is evidenced here by the transition of a broad RF beatnote (cf. Figure 1.4) to a single narrow-band signal. (CF: center frequency)

A more unique and easily observable signature of soliton formation in optical microresonators is the occurrence of discontinuous staircase-like steps in the transmitted pump laser power while the laser is continuously scanned across the optical resonance (cf. Figure 1.7a) [34]². When operating a microresonator a lower pump laser transmission implies a higher average intracavity power. The emergence of the steps may be explained by referring to the cavity bistability curve that describes the power inside the cavity in dependence of the pump laser detuning. When approaching the cavity resonance from the blue detuned side (laser frequency is higher than the resonance frequency and correspondingly laser wavelength is shorter than the resonance wavelength) the intracav-

²Discontinuous steps can also be observed (typically with a higher signal-to-noise ratio) in the power of the nonlinearly generated light.

ity power will increase. This increase of intracavity power will then, due to the Kerr-nonlinearity, effectively shift the resonance frequency towards longer wavelength. As the laser detuning is further decreased the intracavity power will steadily increase (upper branch on the bistability curve), until the highest possible power is reached at the point of effective zero-detuning. Beyond this point (now effectively red-detuned) the intracavity-power will steeply drop to a much lower value (lower branch on the bistability curve) as the Kerr-nonlinearity resonance shift vanishes (cf. Figure 1.8a). Exactly at this transition to red detuning temporal DKS can emerge from the noisy intracavity waveform (cf. Figure 1.9). In this case the formation of a high peak power soliton pulse will cause an additional Kerr-frequency shift such that the part of the pump light that sees the soliton pulse (i.e. copropagating with the soliton inside the cavity) follows now a second bistability curve. 1.8b. The result is a second power drop at a larger detuning when the soliton vanishes.

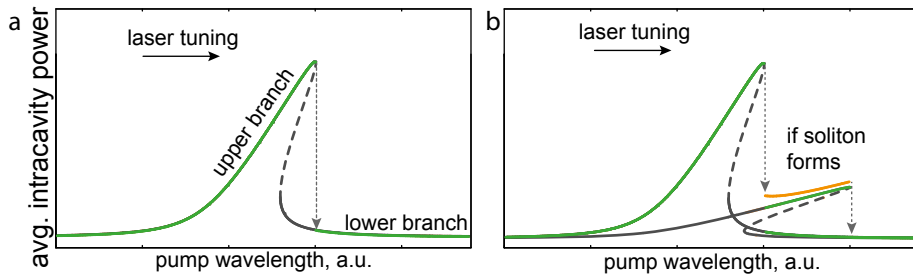


Figure 1.8: Stability of soliton states: Considering only the Kerr-nonlinearity resonance shift the intracavity power can be described by bistability curves where the upper branch solution corresponds to high and the lower branch solution to low intracavity power. When tuning into the resonance with decreasing optical frequency (increasing wavelength) the intracavity power follows the upper branch of the Kerr-bistability curve. After the transition to a soliton state the major fraction of the pump light is described by the lower branch of the bistability curve. The fraction of the pump light that propagates with the soliton inside the microresonator experiences a larger phase shift and is effectively blue detuned on the upper branch of another bistability curve. The extend of the 'soliton bistability curve' towards longer wavelength depends on the peak power of the solitons (i.e. the maximal nonlinear phase shift), the relative height of the curve depends on the relative fraction of the pump light that is affected by the high peak power soliton. The overall intracavity power can be inferred by adding the bistability curves resulting in the black curve.

The combined signal of power drops occurring at different laser detunings leads to the overall staircase-like step structure in the transmitted power. If a higher number of soliton pulses is generated, a series of multiple steps can be observed (during a rapid scan not all solitons disappear at the exact same detuning). The exact number of generated solitons differs from one laser scan to the other as the solitons emerge from a noisy state. It is interesting to note that the transition to effective red-detuning has not been considered in previous work as it is usually associated with only low intracavity power [78]. Section 1.6

will describe how stable operation in the soliton regime can be achieved despite the steps in the intracavity power that can affect the resonator temperature.

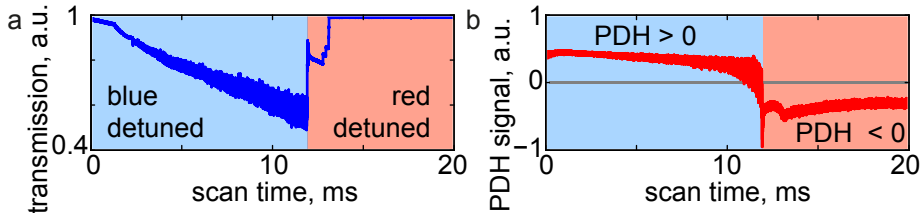


Figure 1.9: Laser detuning and soliton formation. Panel (a) shows the transmitted power and a series of steps associated with multiple temporal Kerr solitons. The background shading indicates the laser detuning that is derived from a Pound-Drever-Hall (PDH) error signal shown in panel (b). The soliton formation coincides with the transition to red detuning (indicated by a sign change in the PDH error signal). Note that the additional Kerr-frequency shift due to the high peak power soliton does not significantly impact the PDH error signal as its relative contribution is small.

1.6 Laser tuning into the Kerr soliton states

For stable operation of a microresonator system thermal self-locking [79, 80] is a widely used method. Here the resonator self-locks itself thermally to the pump laser frequency. Besides being a simple and convenient method, this allows for a fixed pump laser frequency during steady state operation (instead of a pump laser that follows drifts in the resonator). This is advantageous for frequency comb operation, where the pump laser constitutes one of the comb lines that should remain fixed in frequency. The mechanism of thermal self-locking is somewhat analogous to the Kerr-nonlinear bistability curve and gives rise to a so-called thermal triangle, that is known from the earliest reports of whispering-gallery mode microresonators[1, 2]. In a resonator with positive thermo-refractive coefficient (as in MgF_2 or Si_3N_4) thermal locking is achieved by blue detuned pumping. In this regime an increase of pump wavelength (or equivalently a decrease of resonance wavelength) implies a higher intracavity power and higher rate of absorptive heating. As a consequence of this heating and mostly due to the thermo-optic effect the resonance wavelength shifts towards longer wavelength thus stabilizing the relative detuning between pump laser and resonator. Exactly this behavior is present during a soliton state. This can be seen e.g. in Figure 1.7 where (within a particular soliton state) an increase in pump wavelength causes an increase in intracavity power (decrease of transmission).

In order to stably reach the regime of thermal locking of a soliton state it is important that the transition to the soliton state does not induce a change of the resonator temperature (despite the fact that the intracavity power changes), which would directly destabilize the system. One solution to this problem is to tune the pump laser from a far-blue detuned position into the soliton state with a tuning speed chosen such, that the “integrated absorptive heating” over the

tuning time corresponds to the heating rate in the soliton state. In this case the temperature does not change significantly when the soliton state is reached. Thermal locking then ensures the stable operation of the soliton state (for many hours), without actuation on the pump laser frequency, as illustrated in Figure 1.10. It is important to note that the solitons emerge from intrinsic noise present in the cavity prior to reaching the soliton state. As a consequence the initial number of solitons generated via the laser tuning method varies randomly from shot to shot. However, the experimental conditions can often be adjusted such that a certain number of solitons (e.g. one soliton) is generated with high probability. The maximal number of soliton that can be generated via the laser tuning method is related to the dispersion of the cavity and grows with the applied pump power [34]. For typical parameters only a few, maximally up to approximately 10 or 20, solitons are generated. As the exact number depends on a random process the electronically controlled laser tuning method is usually repeated several times until it yields the desired number of solitons. Note that the laser tuning method does not require an

additional external stimulation (e.g. a laser pulse), as it is the case in fiber cavities. The following section will characterize the solitons generated via the described laser tuning method.

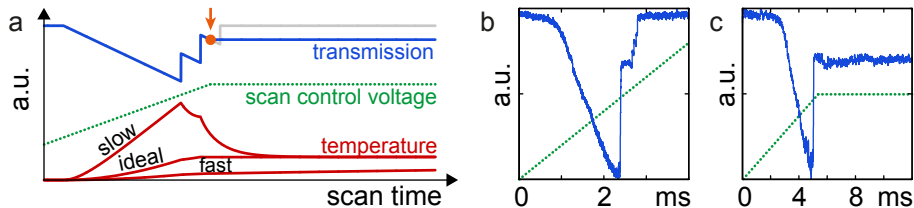


Figure 1.10: Generation of stable solitons via laser tuning. (a) Illustration of laser transmission, scan control voltage (corresponding to pump wavelength) and resonator temperature for slow, ideal and fast laser tuning speed. In the ideal case the resonator temperature does not change once the desired soliton state is reached and the laser scan can be stopped for stable operation. (b) Regular scan of the pump laser over a resonance showing a 'soliton step'. (c) The laser tuning method allows to stop the laser scan once the soliton is generated. Once generated in this manner, the soliton circulates stably inside the microresonator.

1.7 Simulating soliton formation in microresonators

Dissipative temporal Kerr solitons in a microresonator can be simulated by integrating the coupled mode equations (1.11) in time similar to work related to Kerr-combs by [62, 63, 61]. We use an adaptive Runge-Kutta method of the 5-th order, which together with a transformed system of equations without trigonometric functions and explicit time dependence allows achieving fast simulation. The simulation of hundreds of optical lines allows for accurate modeling of realistic experimental systems. This includes in particular the beatnote between the

optical lines (i.e. the repetition rate), the envelope of the optical spectrum as well as instant amplitudes, phases and frequencies of all modes. The sum of the nonlinear mixing terms is efficiently calculated in the Fourier-domain[81]. An additional self-steepening term is added when simulating broad combs in Si_3N_4 rings to better model the behavior of few-cycles pulses[82]. In simulations, similar to the experiment, solitons can be generated via tuning the pump laser into resonance. The number of generated solitons depends on the noisy intracavity waveform preceding the soliton state. To allow for deterministic simulations of a certain number of solitons, the respective number of sech-pulses can be seeded as an initial waveform while the simulation is started directly with a detuning that allows for stable solitons. It is worthwhile noting that the underlying coupled mode equations readily allow for the simulation of complex and irregular mode structures as often encountered in real microresonators (cf. Section 1.9). Based on our simulations we developed an open-source graphical user interface using MATLAB [83] that allows numerical simulation of Kerr-comb and soliton generation in microresonators.

1.8 Characterization of DKS in crystalline microresonators

The ability to stably tune into soliton states as described in the Section 1.6 allows for characterization of the solitons' spectral and temporal properties in crystalline microresonators MgF_2 . Precisely as predicted by theory, the single soliton state has a *sech*-squared spectral envelope from which a pulse duration in the femto-second regime can be inferred. The latter can be confirmed via direct temporal characterization. Here, frequency resolved optical gating using a nonlinear Michelson-interferometer (SHG-FROG)[84] is used, cf. Figure 1.12. This method also allows for the reconstruction of the complex pulse envelope[85]. The high pulse repetition rate inherent to microresonators allows the FROG interferometer delay to extend over several pulse round-trip times, i.e. consecutive pulses can be cross-correlated.

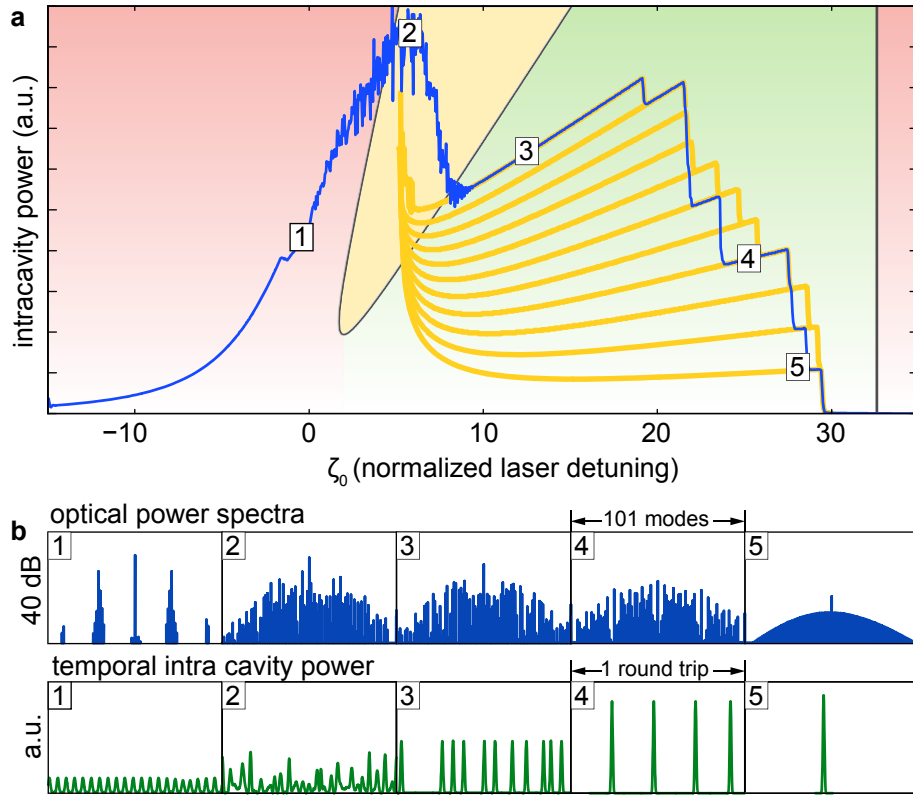


Figure 1.11: Numerical simulations of dissipative Kerr soliton formation in a crystalline microresonator. (a) Intracavity power (corresponding to the transmission signal in Figure 1.7a when mirrored horizontally) during a simulated laser scan (101 simulated modes) over a resonance in a microresonator. The step features are clearly visible. The light gray lines trace out all possible states of the system during the scan. The unshaded area corresponds to the area where temporal DKS can exist, the light shaded area allows for breather solitons with a time variable, oscillating envelope; no solitons can exist in the dark shaded area. b. Optical spectrum and intracavity intensity for different detuning values (1-5) in the laser scan.

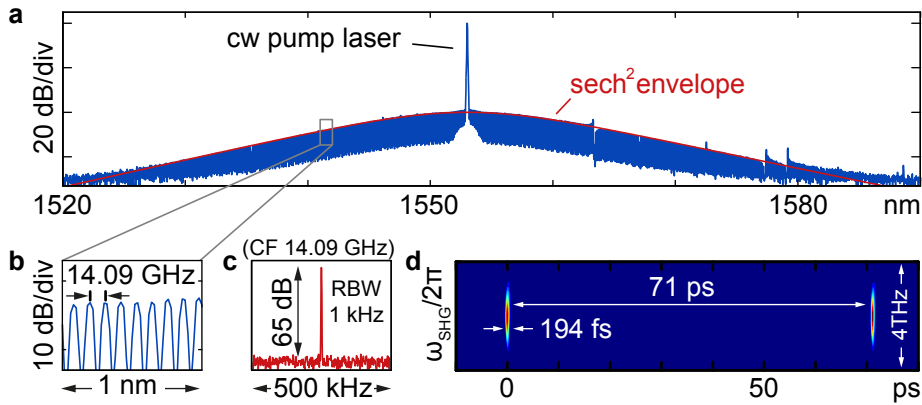


Figure 1.12: Characteristics of a temporal dissipative Kerr soliton in a crystalline resonator. (a) Optical spectrum showing the characteristic sech^2 -envelope. (b) Magnified part of the spectrum, resolving the individual comb lines of which it is composed. (c) The low noise radio-frequency beatnote at 14.09 GHz corresponds to the comb line spacing and the soliton pulse repetition rate. (d) SHG-FROG trace revealing femto-second pulse duration. The pulse to pulse separation of 71 ps corresponds to the pulse repetition rate of 14.09 GHz and the pulse duration of 194 fs can be inferred (in agreement with the spectral width). (RBW: resolution bandwidth, CF: center frequency)

Besides stable single soliton states, also stable multi-soliton states can be generated using the laser tuning method. Figure 1.13 compares the optical spectra and SHG-FROG traces of a single and two different multi-soliton states. A salient feature of multi-soliton states is the modulated spectral envelope arising from the interference of the individual soliton. Based on the spectral envelope the relative positions of the solitons can be reconstructed (cf. Section 1.11). Once a multi-soliton state is generated inside the cavity, the envelope pattern does not change over several hours, implying that the temporal separation between the solitons in the microresonator does not change on this time scale.

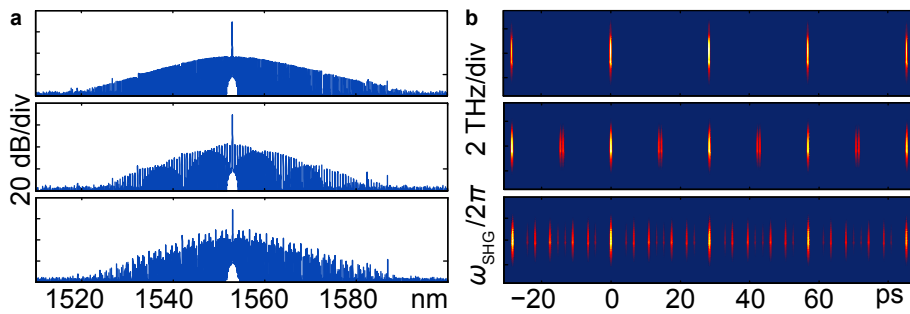


Figure 1.13: Spectral and temporal characterization of multi-soliton states in a crystalline resonator. (a) Optical spectra of a single soliton (top) and two multi-soliton states (middle, bottom). (b) SHG-FROG traces corresponding to (a).

1.9 Resonator mode structure and soliton formation

The generation of bright temporal DKS requires a focusing nonlinearity and an anomalous group velocity dispersion (GVD), i.e. a linear growth of the resonator's FSR with the mode number. In this case the growth of the FSR can be compensated by nonlinear mode pulling, i.e. nonlinear optical shifts of the resonance frequency. In principle most microresonators fulfill this requirement in the (near-) infrared spectral regime. As opposed to optical fiber systems, microresonators, however, can exhibit a rich and complex optical mode structure. Some modes are affected by higher order dispersion or are even characterized by normal GVD. Moreover, fabrication defects and asymmetries can lead to modal coupling and distortions of the mode spectrum due to avoided mode crossings. While temporal dissipative Kerr solitons are a single-mode phenomenon, the structure of the respective mode-family can be altered by the presence of the other modes. The understanding of the impact and influence of the mode-structure is a decisive step in understanding DKS in optical microresonators. In Ref. [35] this is studied experimentally and with the help of the numerical tools described in Section 1.7. First, the mode structure of the microresonator is precisely measured using frequency comb assisted diode laser spectroscopy [86]. Figure 1.14 shows a fraction of the recorded transmission spectrum of a crystalline resonator, revealing several mode families. The full data set is represented in Figure 1.15a. Individual mode families and their dispersion can be extracted from the full data set. An example of a mode family with almost perfect anomalous GVD is shown in Figure 1.15b, top. In contrast, Figure 1.15b, bottom shows another mode family where the globally anomalous GVD is locally modified by two avoided mode crossing. While in the first case solitons can be generated, this is not possible in the latter. The hypothesis that avoided mode crossing (if they occur in the spectral vicinity of the pumped mode) inhibit soliton formation is confirmed by numerical simulation [35]. Moreover, strong higher order dispersion can prevent soliton formation. Importantly, moderate contribution of higher order dispersion and avoided mode crossings further away from the pump wavelength do not inhibit soliton formation but manifest themselves in the optical spectrum as qualitatively illustrated in Figure 1.16. Indeed, similar structures can be observed in the experimentally generated soliton spectra e.g. in Figure 1.12.

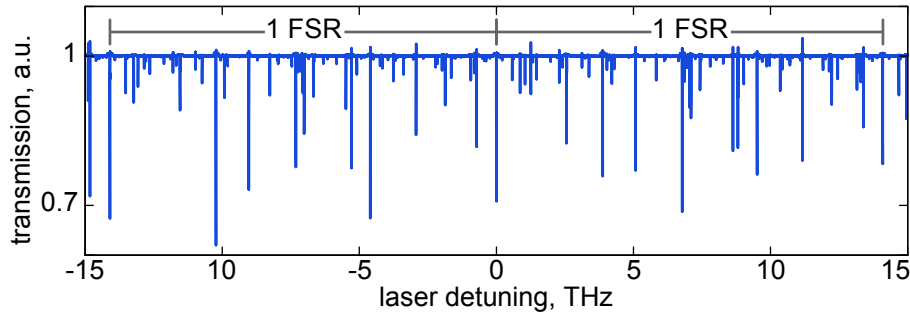


Figure 1.14: Transmission spectrum of a MgF_2 crystalline microresonator with a FSR of approximately 14.09 GHz. The upward transmission spikes (values > 1) result from cavity-ringdown. Frequency comb assisted diode laser spectroscopy ensures precise calibration of the laser detuning (MHz level).

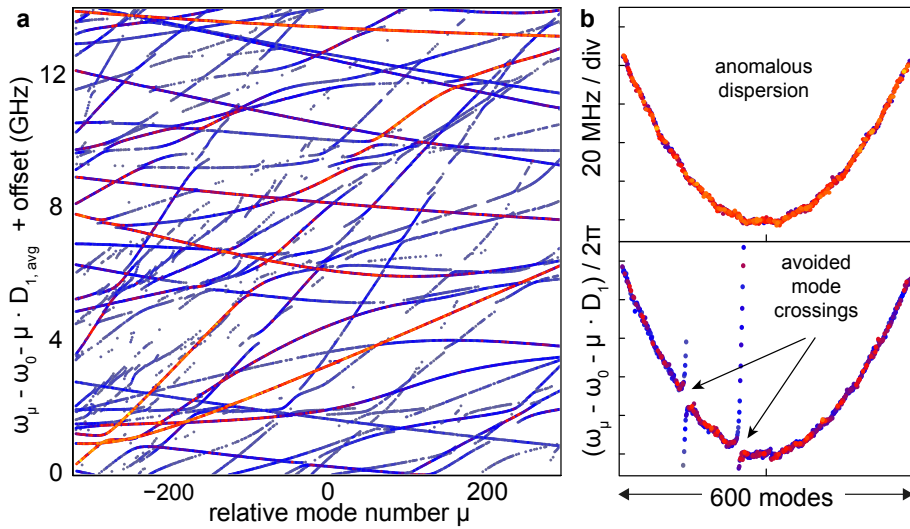


Figure 1.15: Mode structure of a MgF_2 resonator with a FSR of 14.09 GHz. (a) Two-dimensional Echelle-type representation where for all measured mode families the deviation $\omega_\mu - \omega_0 - \mu \cdot D_{1,\text{avg}}$ of the resonance frequency ω_μ from an equidistant $D_{1,\text{avg}}$ -spaced frequency grid ($D_{1,\text{avg}}$ is an approximate average FSR of all modes) is shown (plus some offset) in function of the mode number μ . Dots forming a continuous line represent a particular mode family. Different free spectral ranges correspond to different slopes of the lines, whereas dispersion and variation of the FSR show as curvature and bending of the lines. The dispersion can be strongly affected by mode crossings. (b) Two mode families have been extracted from the data set shown in (a). The upper one is characterized by an anomalous dispersion, the lower one exhibits two avoided mode crossings that induce deviations from the anomalous dispersion.

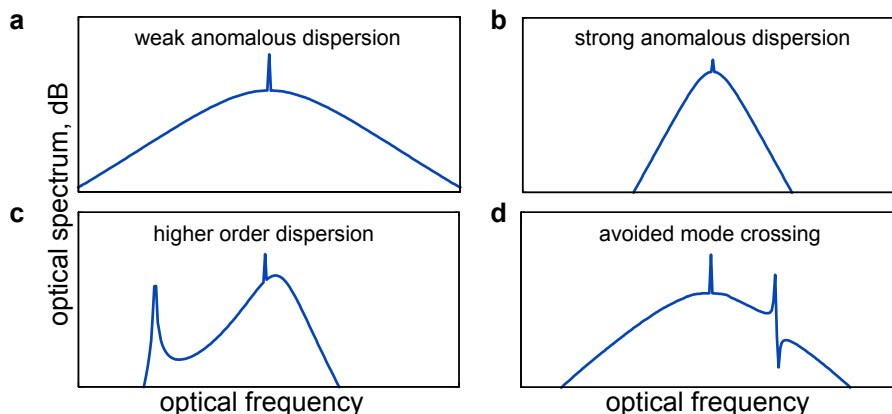


Figure 1.16: Mode-structure and spectral envelope. (a) Typical sech-squared envelope for the case of weak (a) and strong anomalous dispersion (b). (c) Higher order dispersion (such as non zero D_3) leads to an asymmetric spectrum, dispersive wave emission (cf. Section 1.11) and a shift of the spectral soliton peak intensity away from the pump laser (soliton recoil). (d) Avoided mode crossings manifest themselves in a characteristic spectrally local variation of the spectrum.

1.10 Using dissipative Kerr solitons to count the cycles of light

The observation of Kerr solitons in microresonators, and the associated generation of ultra-short femto-second optical pulses, provides an opportunity to count the cycles of light using an optical microresonator, i.e. to link phase coherently an optical laser frequency to the radio frequency domain. In order to achieve such a radio to optical frequency link [87] self-referencing has to be employed; a process where the comb's offset frequency f_0 (cf. Figure 1.1) is measured. To this end, an optical spectrum of sufficient spectral span is required that spans either a full octave when using the $1f$ - $2f$ self-referencing technique or $2/3$ of an octave for the $2f$ - $3f$ self-referencing method [38, 37, 14] (cf. Figure 1.17). While the soliton spectrum generated in a crystalline resonator is not sufficiently broad by itself, the short pulse duration enables (after power amplification in an erbium-doped fiber amplifier) spectral broadening [88] in highly-nonlinear optical fiber. Figure 1.18a shows a soliton spectrum that has been broadened in this way [89]. Here, $2f$ - $3f$ self-referencing is implemented allowing for detection of the soliton comb's offset frequency f_0 (cf. 1.18d). Together, with the comb line spacing (i.e. the pulse repetition rate) f_{rep} that can readily be measured via direct photo-detection (cf. 1.18c), the frequencies constituting the soliton comb are fully defined. In this way, the temporal dissipative Kerr soliton allows linking optical frequencies (e.g. the pump laser wavelength or any other comb line) to the radio (or microwave) frequencies f_0 and f_{rep} .

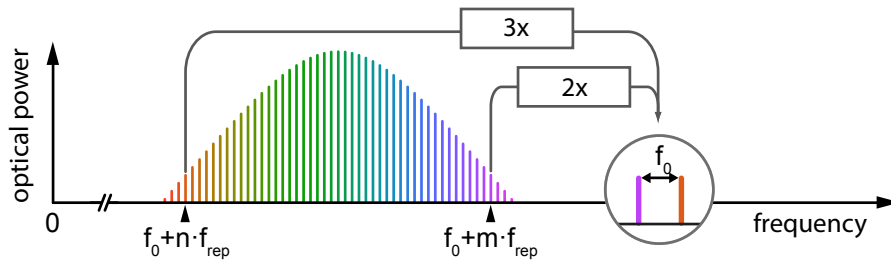


Figure 1.17: Illustration of $2f-3f$ self-referencing. If the frequency comb spectrum spans more than two thirds of an octave, the second and third harmonics of blue and red wings of the spectrum can be overlapped. The difference frequency beatnote between the two harmonics yields the comb's offset frequency f_0 .

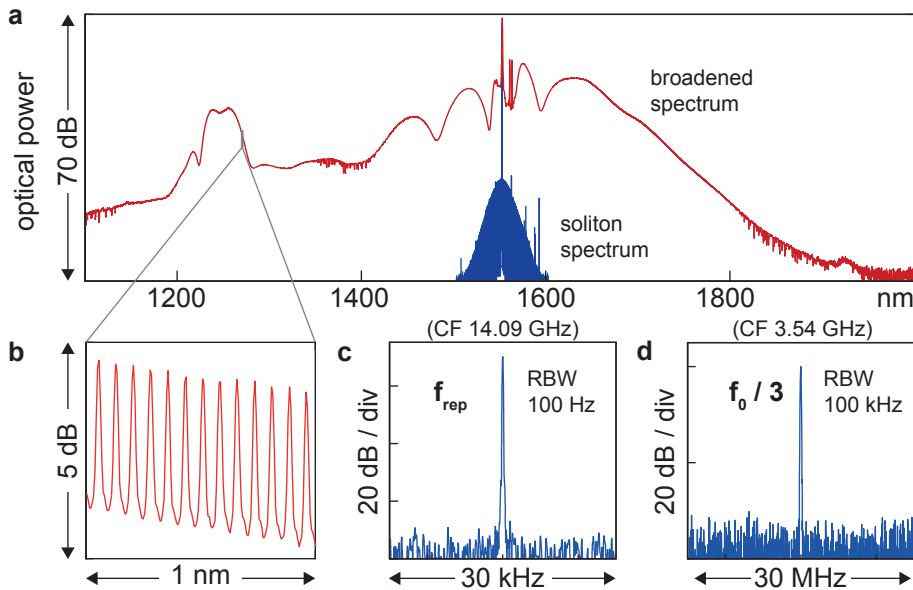


Figure 1.18: Counting the cycles of light by self-referencing a soliton based frequency comb. (a) Soliton spectrum and nonlinearly broadened spectrum. The broadened spectrum spans more than two thirds of an octave and allows for $2f-3f$ self-referencing. (b) Magnified part of the broadened spectrum. The line spacing is the same as for the soliton spectrum (14.09 GHz). (c) Pulse repetition rate beatnote measured via direct photo-detection of the comb spectrum. (d) Offset frequency signal measured via a modified $2f-3f$ self-referencing technique, where two transfer laser are used for signal enhancement (see Ref. [89] for details). (RBW: resolution bandwidth, CF: center frequency)

1.11 Dissipative Kerr solitons and soliton induced Cherenkov radiation in a Si_3N_4 photonic chip

The discovery of temporal DKS in crystalline resonators, as described in the previous chapters not only enables generating coherent optical frequency combs in a reliable manner, but also opened the ability to use time domain broadening methods to achieve a coherent link from the RF (or microwave) domain to the optical frequency domain. A key emerging research question has been if solitons can also be generated in other microresonator platforms. One particularly promising platform for applications are Si_3N_4 integrated microresonators. This platform allows for the integration of coupling waveguide and resonators on a microchip. Indeed, it was demonstrated that by carefully optimizing the fabrication process, the influence of detrimental avoided mode crossings can be strongly reduced, enabling the generation of DKS in Si_3N_4 microresonators[36]. Here, as in the case of crystalline resonators, the soliton formation is indicated by discrete steps in the resonator transmission. Similar to the method described above in detail in Section 1.6 a suitable laser scan allows for stable and thermally locked solitons in Si_3N_4 microresonators. Figure 1.19 shows the generation of a single soliton state in a Si_3N_4 microresonator. The bandwidth of the generated spectrum is much wider than what has been observed in crystalline resonators. As an immediate consequence higher order dispersion terms become relevant; indeed, the third order dispersion causes the Kerr soliton to emit what is known as *Soliton-Cherenkov* radiation[51] (or dispersive wave), i.e. a radiative tail in the time domain. It is important to note that the process can also be understood in the frequency domain as successive FWM [90]. Dispersive wave formation has been predicted particularly for Si_3N_4 resonators, where for a coherent spectrum a spectrally sharp dispersive wave is expected[91], as it is indeed the case (cf. Figure 1.19). For a resonator with third order dispersion (i.e. non-zero D_3), this occurs approximately near the mode number $\mu \approx -3\frac{D_2}{D_3}$ (three times the distance of the zero dispersion point from the pump wavelength, $\mu \approx -\frac{D_2}{D_3}$) [36].

It is important to note that unlike the case of a soliton propagating along an optical fibers where the dispersive wave is generally incoherent with the soliton (i.e. propagating at a velocity different from the soliton's velocity), the coherence can be maintained in case of the microresonator owing to the periodic boundary conditions. This is similar to the coherence of the dispersive wave in supercontinua that are generated by a periodic train of ultra-short pulses. At the same time, the presence of a dispersive wave can also occur in the case of a high noise, non soliton state. The presence of a dispersive wave therefore is not a proof of a coherent Kerr soliton state[92]. Note, that the coherence of the spectrum in Figure 1.19 has been verified by recording the soliton pulse repetition rate beatnote at 190 GHz as well as the heterodyne beatnotes of the soliton spectrum with external CW lasers at various wavelengths (including the dispersive wave spectral region). Based on the spectral width a soliton pulse duration of approximately 30 fs can be estimated.

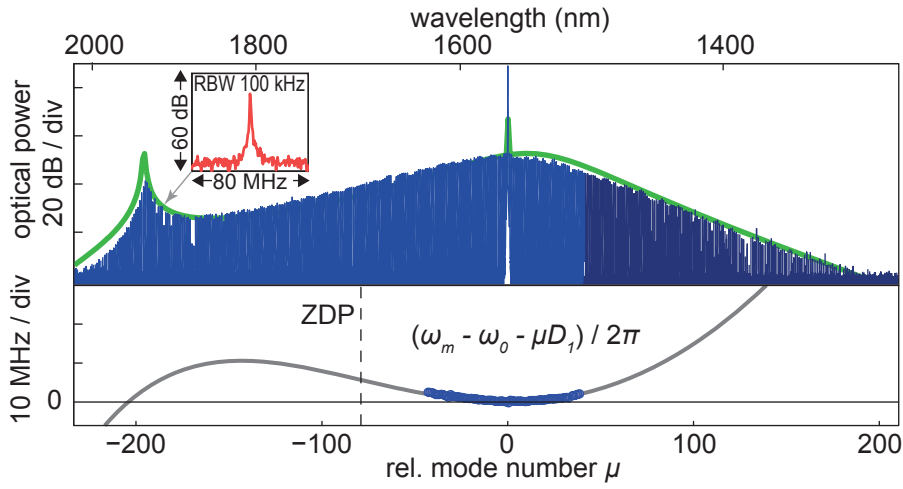


Figure 1.19: Single Kerr soliton generation in a Si_3N_4 microresonator. The upper panel shows the single soliton spectrum that covers a spectral bandwidth of $2/3$ of an octave. The black line in the background is the spectral envelope obtained by the simulation described in Section 1.7. The lower panel shows the measured dispersion (dots) free of avoided mode crossing and the dispersion over the full spectral span as obtained through finite element simulation. The dispersive wave forms at the wavelength of approximately 1.9 micron where the phase matching condition $\omega_\mu - \omega_0 - \mu \cdot D_1 \approx 0$ is fulfilled. The zero dispersion point (ZDP) is marked by a vertical, dashed line. The inset in the upper panel show a heterodyne beatnote between the dispersive wave and an external laser. Its narrow width proves the coherence of the dispersive wave.

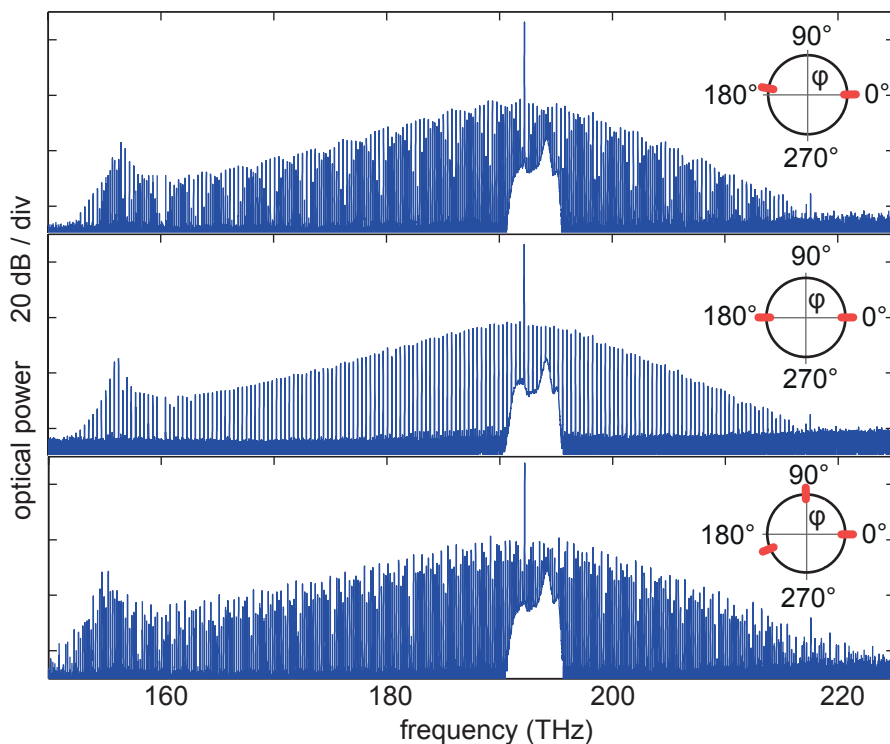


Figure 1.20: Generation of multi-soliton states and soliton induced Cherenkov radiation in a Si_3N_4 microresonator. The characteristic spectral modulations occur due to the interference of solitons at different positions in the microresonators as indicated in the insets.

It is also possible to generate multiple solitons in the Si_3N_4 microresonators. As in the case of the crystalline resonators, once a multi-soliton state is generated, the modulation of the spectral envelope, resulting from the interference of the solitons, remains stable for hours. The spectral envelope function $I(\mu)$ of this interference is given by

$$I(\mu) = \left| \sum_{j=1}^N \exp(i\phi_j \mu) \right|^2,$$

where ϕ_j corresponds to the relative angular position of the j^{th} soliton. From the envelope of the spectrum the single soliton spectrum and the relative positions of the solitons can be reconstructed as shown in Figure 1.20.

1.12 Summary

The observation and stable generation of temporal DKS in optical microresonators provides a major impetus to the field of microresonator frequency combs. It provides a long sought method for the generation of widely spaced frequency combs, with smooth spectral envelope and with low phase noise. In addition,

soliton induced Cherenkov radiation provides a method to increase the bandwidth and transfer the coherence of the comb into the normal GVD regime. Together with the ability to accurately predict the comb performance via numerical simulations, this implies that the synthesis of octave spanning frequency comb spectra directly from a CW laser using a microresonator is a possibility. Solitons in microresonators may make frequency comb metrology ubiquitous by enabling compact comb generators that exhibit mode spacings in the 10 – 100 GHz regime. Potential applications include frequency metrology (i.e. frequency measurements), data transfer, microwave signal generation, spectroscopy, optical sampling and arbitrary optical waveform generation.

Bibliography

- [1] V. B. Braginsky, M. L. Gorodetsky, and V. S. Ilchenko. Quality-factor and nonlinear properties of optical whispering-gallery modes. *Physics Letters A*, 137(7-8):393–397, 1989.
- [2] V. S. Ilchenko and M. L. Gorodetsky. Thermal nonlinear effects in optical whispering gallery microresonators. *Laser Physics*, 2(2):1004–1009, 1992.
- [3] F. Treussart, V. S. Ilchenko, J.-F. Roch, J. Hare, V. Lefèvre-Seguin, J.-M. Raimond, and S. Haroche. Evidence for intrinsic Kerr bistability of high-Q resonators in suprafluid helium. *European Physical Journal D*, 1:235–238, 1998.
- [4] S. M. Spillane, T. J. Kippenberg, and K. J. Vahala. Ultralow-threshold Raman laser using a spherical dielectric microcavity. *Nature*, 415(6872):621–623, 2002.
- [5] I. S. Grudinin, A. B. Matsko, and L. Maleki. Brillouin lasing with a CaF₂ whispering gallery mode resonator. *Physical Review Letters*, 102:43902, 2009.
- [6] D. A. Cohen, M. Hossein-Zadeh, and A. F. J. Levi. High-Q microphotonic electro-optic modulator. *Solid-State Electronics*, 45:1577–1589, 2001.
- [7] V. S. Ilchenko, A. A. Savchenkov, A. B. Matsko, and L. Maleki. Whispering-gallery-mode electro-optic modulator and photonic microwave receiver. *Journal of the Optical Society of America B-Optical Physics*, 20:333–342, 2003.
- [8] V. S. Ilchenko, A. A. Savchenkov, A. B. Matsko, and L. Maleki. Nonlinear optics and crystalline whispering gallery mode cavities. *Physical Review Letters*, 92(4):43903, 2004.
- [9] T. Carmon and K. J. Vahala. Visible continuous emission from a silica microphotonic device by third-harmonic generation. *Nature Physics*, 3(6):430–435, June 2007.
- [10] D. N. Klyshko. *Photons and Nonlinear Optics*. Gordon and Breach Science Publishers, 1988.
- [11] T. J. Kippenberg, S. M. Spillane, and K. J. Vahala. Kerr-nonlinearity optical parametric oscillation in an ultrahigh-Q toroid microcavity. *Physical Review Letters*, 93(8):83904, 2004.

- [12] A. A. Savchenkov, A. B. Matsko, D. Strekalov, M. Mohageg, V. S. Ilchenko, and L. Maleki. Low threshold optical oscillations in a whispering gallery mode CaF₂ resonator. *Physical Review Letters*, 93:243905, 2004.
- [13] P Del’Haye, A Schliesser, O Arcizet, T Wilken, R Holzwarth, and T Kippenberg. Optical frequency comb generation from a monolithic microresonator. *Nature*, 450:1214–1217, 2007.
- [14] Th. Udem, R. Holzwarth, and T. W. Hänsch. Optical frequency metrology. *Nature*, 416:233–237, 2002.
- [15] S. T. Cundiff and J. Ye. Colloquium: Femtosecond optical frequency combs. *Reviews of Modern Physics*, 75(1):325, 2003.
- [16] A. A. Savchenkov, A. B. Matsko, V. S. Ilchenko, I. Solomatine, D. Seidel, and L. Maleki. Tunable optical frequency comb with a crystalline whispering gallery mode resonator. *Physical Review Letters*, 101(9):93902, August 2008.
- [17] M. A. Foster, J. S. Levy, O. Kuzucu, K. Saha, M. Lipson, and A. L. Gaeta. Silicon-based monolithic optical frequency comb source. *Opt. Express*, 19(15):14233–14239, July 2011.
- [18] J. S. Levy, A. Gondarenko, M. A. Foster, A. C. Turner-Foster, A. L. Gaeta, and M. Lipson. CMOS-compatible multiple-wavelength oscillator for on-chip optical interconnects. *Nature Photonics*, 4(1):37–40, January 2010.
- [19] L. Razzari, D. Duchesne, M. Ferrera, R. Morandotti, S. Chu, B. E. Little, and D. J. Moss. CMOS-compatible integrated optical hyper-parametric oscillator. *Nature Photonics*, 4(1):41–45, January 2010.
- [20] D. J. Moss, R. Morandotti, A. L. Gaeta, and M. L. Lipson. New CMOS-compatible platforms based on silicon nitride and Hydex for nonlinear optics. *Nature Photonics*, 7:597–563, 2013.
- [21] H. Jung, K. Y. Xiong, C. and Fong, X. Zhang, and H. X. Tang. Optical frequency comb generation from aluminum nitride microring resonator. *Optics Letters*, 38(15):2810–2813, 2013.
- [22] B. J. M. Hausmann, I. Bulu, V. Venkataraman, P. Deotare, and M. Loncar. Diamond nonlinear photonics. *Nature Photonics*, 8(5):369–374, 2014.
- [23] P. Del’Haye, O. Arcizet, A. Schliesser, R. Holzwarth, and T. J. Kippenberg. Full stabilization of a microresonator-based optical frequency comb. *Physical Review Letters*, 101(5):053903, 2008.
- [24] A. R. Johnson, Y. Okawachi, J. S. Levy, J. Cardenas, K. Saha, M. Lipson, and A. L. Gaeta. Chip-based frequency combs with sub-100 GHz repetition rates. *Opt. Lett.*, 37(5):875–877, March 2012.
- [25] J. Pfeifle, V. Brasch, M. Laueremann, Y. Yu, D. Wegner, T. Herr, K. Hartinger, Ph. Schindler, J. Li, D. Hillerkuss, R. Schmogrow, C. Weimann, R. Holzwarth, W. Freude, J. Leuthold, T. J. Kippenberg, and C. Koos. Coherent terabit communications with microresonator Kerr frequency combs. *Nature Photonics*, 8(5):375–380, 2014.

- [26] T. Steinmetz, T. Wilken, C. Araujo-Hauck, R. Holzwarth, T. W. Hänsch, L. Pasquini, A. Manescau, S. D’Odorico, M. T. Murphy, T. Kenitscher, W. Schmidt, and T. Udem. Laser frequency combs for astronomical observations. *Science*, 321:1335–1337, 2008.
- [27] M. T. Murphy, T. Udem, R. Holzwarth, A. Sismann, L. Pasquini, C. Araujo-Hauck, H. Dekker, S. D’Odorico, M. Fischer, T. W. Hansch, and A. Manescau. High-precision wavelength calibration of astronomical spectrographs with laser frequency combs. *Monthly Notices Of The Royal Astronomical Society*, 380(2):839–847, September 2007.
- [28] A. A. Savchenkov, E. Rubiola, A. B. Matsko, V. S. Ilchenko, and L. Maleki. Phase noise of whispering gallery photonic hyper-parametric microwave oscillators. *Optics Express*, 16(6):4130–4144, March 2008.
- [29] J. Li, H. Lee, T. Chen, and K. J. Vahala. Low-pump-power, low-phase-noise, and microwave to millimeter-wave repetition rate operation in microcombs. *Phys. Rev. Lett.*, 109(23):233901, August 2012.
- [30] Z. Jiang, C. B. Huang, D. E. Leaird, and A. M. Weiner. Optical arbitrary waveform processing of more than 100 spectral comb lines. *Nature Photonics*, 1(8):463–467, August 2007.
- [31] I. V. Barashenkov and Yu. S. Smirnov. Existence and stability chart for the ac-driven, damped nonlinear Schrödinger solitons. *Phys. Rev. E*, 54(5):5707–5725, November 1996.
- [32] S. Wabnitz. Suppression of interactions in a phase-locked soliton optical memory. *Opt. Lett.*, 18(8):601–603, April 1993.
- [33] F. Leo, S. Coen, P. Kockaert, S.-P. P. Gorza, P. Emplit, and M. Haelterman. Temporal cavity solitons in one-dimensional Kerr media as bits in an all-optical buffer. *Nature Photonics*, 4(7):471–476, July 2010.
- [34] T. Herr, V. Brasch, J. D. Jost, C. Y. Wang, N. M. Kondratiev, M. L. Gorodetsky, and T. J. Kippenberg. Temporal solitons in optical microresonators. *Nature Photonics*, 8(2):145–152, December 2013.
- [35] T. Herr, V. Brasch, J. D. Jost, I. Mirgorodskiy, G. Lihachev, M. L. Gorodetsky, and T. J. Kippenberg. Mode spectrum and temporal soliton formation in optical microresonators. *Physical Review Letters*, 113(12):123901, September 2014.
- [36] V. Brasch, T. Herr, M. Geiselmann, G. Lihachev, M. H. P. Pfeiffer, M. L. Gorodetsky, and T. J. Kippenberg. Photonic chip based optical frequency comb using soliton induced Cherenkov radiation. *arXiv*, 1410.8598, 2014.
- [37] J. Reichert, R. Holzwarth, T. Udem, and T. W. Hänsch. Measuring the frequency of light with mode-locked lasers. *Optics Communications*, 172:59–68, 1999.
- [38] H. R. Telle, G. Steinmeyer, A. E. Dunlop, J. Stenger, D. H. Sutter, and U. Keller. Carrier-envelope offset phase control: A novel concept for absolute optical frequency measurement and ultrashort pulse generation. *Applied Physics B-Lasers And Optics*, 69(4):327–332, October 1999.

- [39] T. M. Ramond, S. A. Diddams, L. Hollberg, and A. Bartels. Phase-coherent link from optical to microwave frequencies by means of the broadband continuum from a 1-GHz Ti:sapphire femtosecondoscillator. *Optics Letters*, 27(20):1842, October 2002.
- [40] I. H. Agha, Y. Okawachi, M. A. Foster, J. E. Sharping, and A. L. Gaeta. Four-wave-mixing parametric oscillations in dispersion-compensated high- $\{Q\}$ silica microspheres. *Physical Review A*, 76:43837, 2007.
- [41] I. H. Agha, Y. Okawachi, and A. L. Gaeta. Theoretical and experimental investigation of broadband cascaded four-wave mixing in high- Q microspheres. *Optics Express*, 17(18):16209–16215, August 2009.
- [42] A. C. Turner, M. A. Foster, A. L. Gaeta, and M. Lipson. Ultra-low power parametric frequency conversion in a silicon microring resonator. *Optics Express*, 16(7):4881–4887, March 2008.
- [43] V. S. Ilchenko, X. S. Yao, and L. Maleki. Microsphere integration in active and passive photonics devices. In A. V. Kudryashov and A. H. Paxton, editors, *Laser Resonators III*, volume 3930 of *Proceedings of the Society of Photo-Optical Instrumentation Engineers (Spie)*, pages 154–162, 2000.
- [44] A. A. Savchenkov, V. S. Ilchenko, A. B. Matsko, and L. Maleki. Kilo-hertz optical resonances in dielectric crystal cavities. *Physical Review A*, 70(5):051804, 2004.
- [45] A. A. Savchenkov, A. B. Matsko, V. S. Ilchenko, and L. Maleki. Optical resonators with ten million finesse. *Optics Express*, 15:6768, 2007.
- [46] D. K. Armani, T. J. Kippenberg, S. M. Spillane, and K. J. Vahala. Ultra-high- Q toroid microcavity on a chip. *Nature*, 421:925–928, 2003.
- [47] J. C. Knight, G. Cheung, F. Jacques, and T. A. Birks. Phase-matched excitation of whispering-gallery-mode resonances by a fiber taper. *Optics Letters*, 22(15):1129–1131, 1997.
- [48] S. M. Spillane, T. J. Kippenberg, O. J. Painter, and K. J. Vahala. Ideality in a fiber-taper-coupled microresonator system for application to cavity quantum electrodynamics. *Physical Review Letters*, 91(4):43902, 2003.
- [49] J. S. Levy, A. Gondarenko, M. A. Foster, A. C. Turner-Foster, A. L. Gaeta, and M. Lipson. Monolithically integrated multiple wavelength oscillator on silicon. *arXiv:0907.1077*, 2009.
- [50] T. Herr, K. Hartinger, J. Riemensberger, C. Y. Wang, E. Gavartin, R. Holzwarth, M. L. Gorodetsky, and T. J. Kippenberg. Universal formation dynamics and noise of Kerr-frequency combs in microresonators. *Nature Photonics*, 6(June):480–487, 2012.
- [51] N. Akhmediev and M. Karlsson. Cherenkov radiation emitted by solitons in optical fibers. *Physical Review A*, 51(3):2602–2607, 1995.
- [52] V. Brasch, Q.-F. Chen, S. Schiller, and T. J. Kippenberg. Radiation hardness of high- q silicon nitride microresonators for space compatible integrated optics. *arXiv*, 1406.0297, 2014.

- [53] P. Del’Haye, T. Herr, E. Gavartin, M. L. Gorodetsky, R. Holzwarth, and T. J. Kippenberg. Octave spanning tunable frequency comb from a microresonator. *Physical Review Letters*, 107(6):063901, 2011.
- [54] F. Ferdous, H. Miao, D. E. Leaird, K. Srinivasan, J. Wang, L. Chen, L. T. Varghese, and A. M. Weiner. Spectral line-by-line pulse shaping of on-chip microresonator frequency combs. *Nature Photonics*, 5:770–776, December 2011.
- [55] Y. Okawachi, K. Saha, J. S. Levy, Y. H. Wen, M. Lipson, and A. L. Gaeta. Octave-spanning frequency comb generation in a silicon nitride chip. *Optics Letters*, 36(17):3398–3400, September 2011.
- [56] P Del’Haye, K. Beha, S. B. Papp, and S. A. Diddams. Self-injection locking and phase-locked states in microresonator-based optical frequency combs. *Physical Review Letters*, 112(4):043905, January 2014.
- [57] T. Herr, V. Brasch, J. D. Jost, C. Y. Wang, N. M. Kondratiev, M. L. Gorodetsky, and T. J. Kippenberg. Mode-locking in an optical microresonator via soliton formation. *arXiv*, 1211.0733, November 2012.
- [58] A. B. Matsko, A. A. Savchenkov, D. Strekalov, V. S. Ilchenko, and L. Maleki. Optical hyperparametric oscillations in a whispering-gallery-mode resonator: Threshold and phase diffusion. *Physical Review A*, 71:33804, 2005.
- [59] L. Maleki, V. S. Ilchenko, A. A. Savchenkov, W. Liang, D. Seidel, and A. B. Matsko. High performance, miniature hyper-parametric microwave photonic oscillator. In *Frequency Control Symposium (FCS), 2010 IEEE International*, pages 558–563, 2010.
- [60] A. B. Matsko, A. A. Savchenko, W. Liang, V. S. Ilchenko, D. Seidel, and L Maleki. Mode-locked Kerr frequency combs. *Optics Letters*, 36:2845–2847, 2011.
- [61] Y. K. Chembo, D. V. Strekalov, and N. Yu. Spectrum and dynamics of optical frequency combs generated with monolithic whispering gallery mode resonators. *Physical Review Letters*, 104(10):103902, March 2010.
- [62] Y. K. Chembo and N. Yu. Modal expansion approach to optical-frequency-comb generation with monolithic whispering-gallery-mode resonators. *Phys. Rev. A*, 82(3):33801, September 2010.
- [63] Y. K. Chembo and N. Yu. On the generation of octave-spanning optical frequency combs using monolithic whispering-gallery-mode microresonators. *Optics Letters*, 35(16):2696–2698, August 2010.
- [64] R. W. Boyd. *Nonlinear Optics*. Academic Press, 3ed., 2007.
- [65] M. L. Gorodetsky and A. E. Fomin. Eigenfrequencies and Q-factor in the geometrical theory of whispering-gallery modes. *Quantum Electronics*, 37(2):167–172, February 2007.
- [66] M. L. Gorodetsky. *Optical Microresonators with Giant Quality-Factor*. Moscow, Fizmatlit (in Russian), 2011.

- [67] Y. A. Demchenko and M. L. Gorodetsky. Analytical estimates of eigenfrequencies, dispersion, and field distribution in whispering gallery resonators. *Journal of the Optical Society of America B-Optical Physics*, 30(11):3056–3063, 2013.
- [68] C. Y. Bao and C. X. Yang. Quantitative analysis of the mode-pulling effect in microcomb generation based on the modal expansion method. *Journal of the Optical Society of America B-Optical Physics*, 30:3243–3248, 2013.
- [69] W. B. Whitten, M. D. Barnes, and J. M. Ramsey. Propagation of short optical pulses in a dielectric sphere. *Journal of the Optical Society of America B-Optical Physics*, 14:3424–3429, 1997.
- [70] A. B. Matsko, A. A. Savchenkov, W. Liang, V. S. Ilchenko, D. Seidel, and L. Maleki. Whispering gallery mode oscillators and optical comb generators. In *Proceedings of the 7th Symposium Frequency Standards and Metrology*, pages 539–558, 2009.
- [71] Y. K. Chembo and C. R. Menyuk. Spatiotemporal Lugiato-Lefever formalism for Kerr-comb generation in whispering-gallery-mode resonators. *Physical Review A*, 87(5):053852, May 2013.
- [72] L. A. Lugiato and R. Lefever. Spatial dissipative structures in passive optical systems. *Physical Review Letters*, 21:2209–2211, 1987.
- [73] V. E. Zakharov and A. B. Shabat. Exact theory of two-dimensional self-focusing and one-dimensional self-modulation of waves in nonlinear media (differential equation solution for plane self focusing and one dimensional self modulation of waves interacting in nonlinear media). *Soviet Physics-JETP*, 34:62–69, 1972.
- [74] D. Anderson. Variational approach to non-linear pulse-propagation in optical fibers. *Physical Review A*, 27(6):3135–3145, 1983.
- [75] F. G. Mertens, N. R. Quintero, and A. R. Bishop. Nonlinear schrodinger equation with spatiotemporal perturbations. *Physical Review E*, 81, 2010.
- [76] A. Coillet, I. Balakireva, R. Henriet, K. Saleh, L. Larger, J. M. Dudley, C. R. Menyuk, and Y. K. Chembo. Azimuthal turing patterns, bright and dark cavity solitons in kerr combs generated with whispering-gallery-mode resonators. *IEEE Photonics Journal*, 5:9, 2013.
- [77] A. Matsko, A. Savchenko, and L. Maleki. On excitation of breather solitons in an optical microresonator. *Optics Letters (early posting)*, 2012.
- [78] T. Carmon, L. Yang, and K. J. Vahala. Dynamical thermal behavior and thermal selfstability of microcavities. *Optics Express*, 12:4742–4750, 2004.
- [79] T. Carmon, H. G. L. Schwefel, L. Yang, M. Oxborrow, A. D. Stone, and K. J. Vahala. Static envelope patterns in composite resonances generated by level crossing in optical toroidal microcavities. *Physical Review Letters*, 100(10):103905, March 2008.

- [80] J. Li, S. Diddams, and K. J. Vahala. Pump frequency noise coupling into a microcavity by thermo-optic locking. *Optics Express*, 22(12):14559–14567, 2014.
- [81] T. Hansson, D. Modotto, and S. Wabnitz. On the numerical simulation of Kerr frequency combs using coupled mode equations. *Optics Communications*, 312:134–136, 2014.
- [82] M. R. E. Lamont, Y. Okawachi, and A. L. Gaeta. Route to stabilized ultrabroadband microresonator-based frequency combs. *Optics Letters*, 38(18):3478–81, September 2013.
- [83] G. V. Lihachev, T. Herr, T. J. Kippenberg, and M. L. Gorodetsky. Tool for simulation of kerr frequency combs. In *Microresonator Frequency Combs and Applications*, Ascona, Switzerland, 2009. (code: <http://www.rqc.ru/groups/gorodetsky/combgui.htm>).
- [84] D. J. Kane and R. Trebino. Characterization of arbitrary femtosecond pulses using frequency-resolved optical gating. *IEEE Journal of Quantum Electronics*, 29(2):571–579, 1993.
- [85] D. J. Kane. Principal components generalized projections: a review. *J. Opt. Soc. Am. B*, 25(6):A120—A132, June 2008.
- [86] P. Del’Haye, O. Arciezt, M. L. Gorodetsky, R. Holzwarth, and T. J. Kippenberg. Frequency comb assisted diode laser spectroscopy for measurement of microcavity dispersion. *Nature Photonics*, pages 529–533, 2009.
- [87] S. A. Diddams, D. J. Jones, J. Ye, S. T. Cundiff, J. L. Hall, J. K. Ranka, R. S. Windeler, R. Holzwarth, T. Udem, and T. W. Hänsch. Direct link between microwave and optical frequencies with a 300 THz femtosecond laser comb. *Physical Review Letters*, 84:5102–5105, 2000.
- [88] J. M. Dudley, G. Genty, and S. Coen. Supercontinuum generation in photonic crystal fiber. *Reviews of Modern Physics*, 78(4):1135–1184, 2006.
- [89] J. D. Jost, T. Herr, C. Lecaplain, V. Brasch, M. H. P. Pfeiffer, and T. J. Kippenberg. Microwave to optical link using an optical microresonator. *arXiv*, 1411.1354, 2014.
- [90] M. Erkintalo, Y. Q. Xu, S. G. Murdoch, J. M. Dudley, and G. Genty. Cascaded phase matching and nonlinear symmetry breaking in fiber frequency combs. *Physical Review Letters*, 109(22):223904, November 2012.
- [91] S. Coen, H. G. Randle, T. Sylvestre, and M. Erkintalo. Modeling of octave-spanning Kerr frequency combs using a generalized mean-field Lugiato-Lefever model. *Opt. Lett.*, 38(1):37–39, 2013.
- [92] M. Erkintalo and S. Coen. Coherence properties of Kerr frequency combs. *Optics Letters*, 39:283–286, 2014.